

https://dspace.org/

Fracture of plain concrete: a comparative study of notched beams of varying depth

Alexander, Mark Gavin

2014-09-12
http://hdl.handle.net/10539/15527

Downloaded from a DSpace repository. https://dspace.org/

It should be noted that some inaccuracy in compliance measurements has been introduced by the fact that firstly the load was not always removed immediately the peak load for the cycle was achieved (i.e. some additional crack growth could have occurred before unloading) and secondly δ_p was influenced by creep during the time taken to record strains. Both of these effects can be noted in figure 6.1. The effect of these inaccuracies is to cause conventional compliances to be slightly underestimated, and to somewhat increase the area under the load-deflection curve. The magnitude of the inaccuracies were considered to be small relative to the scatter of results.

6.7 SLOW CRACK GROWTH IN FRACTURE BEAMS

The compliance method outlined previously may be used to assess slow crack growth during a test. However, in cemented materials the problem exists of defining exactly what is meant by crack growth. This might be visible crack growth, or development of a microcracked zone, or increase in effective crack depth (where effective crack depth is the sum of stress-free crack depth and the depth of the microcracked zone). At this point, we do not yet have a reasonable estimate of the depth of the microcracked zone, and therefore it is proposed to use the concept of "apparent" crack depth introduced in 6.6.2. This is the crack depth inferred from the conventional compliance relationship using measured compliance changes. This apparent crack depth will generally be longer than the visible crack depth but shorter than the effective crack depth, as was shown in figure 6.4. Accepting this limitation, it is nevertheless true that the apparent crack depth will give some physical measure of the extent of crack growth during a test, and will allow us to compare the behaviour of different beam sizes.

In this section, the apparent crack growth occurring at maximum load will be examined, since this point is often used to assess fracture parameters. Many investigators have assumed that no crack growth

occurs prior to maximum load, but the beams of series F3 have clearly shown this assumption to be erroneous. It has also been suggested that crack growth in larger specimens will be less than in smaller specimens, thus causing larger specimens to yield more valid estimates of LEFM parameters. Results of the present tests show, however, that while relative crack growth in larger beams may be less than in smaller beams, it is by no means negligible.

For the purposes of this section, the apparent crack growth prior to peak load will be termed Δc, so that at maximum load:-

$$c_c = c_0 + \Delta c \qquad (6.5)$$

where c_c is the apparent critical crack depth at maximum load and c_0 is the initial notch depth. We may also define the initial residual ligament depth as:-

$$h_0 = d - c_0 \qquad (6.6)$$

6.7.1 VISIBLE CRACK GROWTH AT MAXIMUM LOAD (SERIES F3)

The beams of series F3 generally showed visible crack growth during the maximum load cycle. In those beams in which no visible crack growth could be observed at maximum load, it was also noticed that compliances were somewhat less than those experienced by beams with visible crack growth (see for instance figure 6.3(a)). In view of the difficulty of detecting crack growth visually in smaller beams, it was debatable whether crack growth had occurred in these or not. However, the weight of evidence seems to suggest that main crack extension did occur before maximum load.

Crack growth at maximum load was detected in 14 of the 23 beams of series F3 that were monitored for crack growth. The results are shown in figure 6.9 in the form of bar diagrams giving the range

of crack growth values for the particular beam types. A scatter of results is again inevitable, but the general trend is that of increasing crack growth with increasing beam size. Ultimately it is not the absolute crack growth that is important, but rather the relative crack growth, and this will be discussed below.

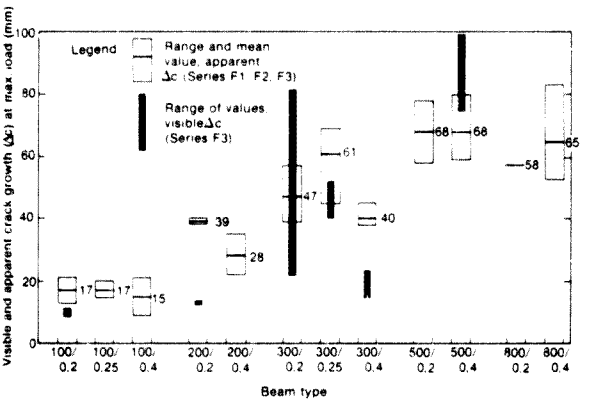

Figure 6.9 Crack growth at maximum load (series F3)

6.7.2 APPARENT CRACK GROWTH AT MAXIMUM LOAD (SERIES F1, F2, F3)

Apparent crack growth (Δc) using the compliance method was assessed for beams of all three series. (Note that the 100x100x850mm (0,5) beams of series F2 were excluded since certain of the beams had initial linear portions that were unrepresentative of true behaviour, and the definition of the peak load as the point of fracture instability was questionable due to the flat peaks and obvious absence of any degree of spontaneous crack growth). These results are presented in bar diagram form showing absolute Δc in figure 6.9, and in graphical form showing relative values (i.e. $\Delta c/c_0$) in figure 6.10. Comment on the figures is as follows:-

FIGURE 6.9

As might be expected, the absolute value of crack extension at maximum load increases as beam depth increases. Subject to the limited number of results for larger beams (500mm and 800mm), the general trend is that crack extension for any beam size is independent of initial notch-depth ratio. Since the compliance curves (figure 6.3) are continuously increasing, this implies that compliance changes at maximum load will be larger for deeper notched beams than shallower notched ones. Visible and apparent crack growths can also be compared in figure 6.9. It is interesting that for those 100mm and 200mm beams where visible crack growth could be detected, this is less than apparent crack growth. This critically affects calculated fracture parameters, as discussed later in chapter 9. For the larger beams, however, the visible crack growth roughly matches the apparent crack growth.

FIGURE 6.10

Whereas absolute crack growth reduces with beam depth, the opposite trend is shown for relative crack growth ($\Delta c/c_0$). This trend is consistent for both shallow and deep notching. For the 500mm beams, $\Delta c/c_0$ values are about 0,2 for $c_0/d = 0,4$, whereas in the shallow-notched small beams these values are as high as 1,0, indicating that the initial notch depth is doubled prior to maximum load. However, it will be shown in chapter 9 that crack growth for 100mm beams can be seriously overestimated using conventional compliance relationships. Figure 6.10 is essentially a reflection of figure 6.5; the greater compliances of the smaller beams may be interpreted as being due to lower restraint in the fracture zone.

Figure 6.10 also explores the possibility of a relationship between slow crack growth $\Delta c/c_0$ and initial residual ligament depth h_0. A fairly linear trend is evident in which $\Delta c/c_0$ may be considered to depend more or less linearly on h_0, with different relationships

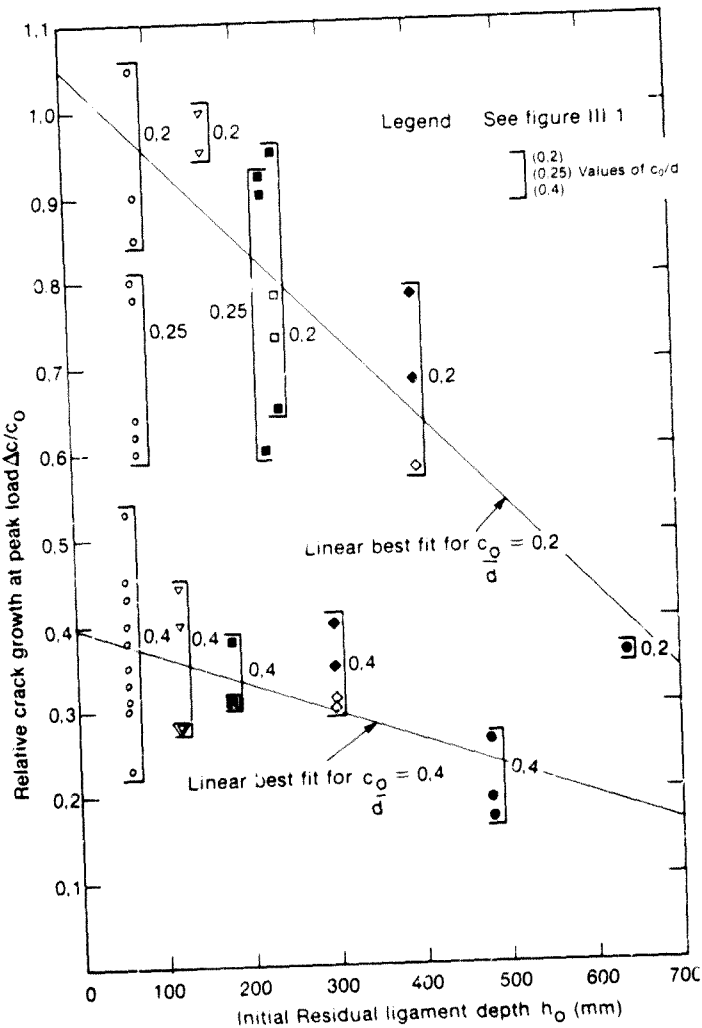

Figure 6.10 Relationship between slow crack growth, initial notch depth ratio, and initial residual ligament depth

depending on initial notch depth ratio. Insufficient results are available for $c_0/d = 0,25$ to suggest a relationship for this notch depth. For the material tested, slow crack growth may be assessed simply from a knowledge of beam and notch dimensions (i.e. c_0 and h_0). This procedure in itself would simplify the compliance approach and give at least a first estimate of likely crack growth which would be useful in assessing fracture loads.

The figure also shows that the sensitivity of slow crack growth to beam size decreases as the notching becomes deeper i.e. a greater degree of relative crack growth for any beam size will occur if the beam has a shallow notch. This implies that structures such as concrete road slabs where the starter flaws may be fairly small will experience considerable crack growth prior to final failure. Figure 6.10 also indicates that, since less relative slow crack growth occurs in deep beams, the condition of a truly brittle Griffith-type material is more closely approached for these beams.

Many researchers have argued that deep sections are required for obtaining valid fracture parameters, but frequently such arguments have ignored the effects of slow crack growth prior to instability. Clearly in such cases, tests on larger beams will produce fracture parameters closer to "true" values simply because slow crack growth is reduced in these beams, and the consequences of ignoring this effect will be less serious than in small beams. Nevertheless in spite of the deep sections tested here, slow crack growth was not negligible, and amounted in relative terms to as much as one-quarter of the initial notch depth. This is clear evidence of the importance of assessing slow crack growth in cemented materials.

6.8 CONCLUSIONS

1. Compliance relationships for cemented materials are complicated by the presence of a microcracked fracture zone in which

crack-closing stresses operate. Theoretical relationships that ignore this effect are therefore not entirely valid.

2. Using experimental load-deflection curves, it is possible to define two compliances:- the conventional compliance which is simply the inverse slope of a line joining the origin to the point (F,δ) in question; and the modified compliance which is a reloading compliance obtained from the inverse of the slope of the linear portion of the reloading curve in any load cycle. The presence of the microcracked zone as well as irrecoverable deformation influences these compliances.

3. Initial notch compliances of the fracture beams agree well with theory. This is before any non-linearity and damage occurs.

4. Considerable irrecoverable deformation occurs, resulting from resistance to crack closing which is due to previous aggregate pull-out and crack surface disintegration.

5. Experimental compliance relationships based on visible crack growth show that the fracture beams are more compliant than theory would predict; this is to be expected due to the development of a microcracked zone which reduces the stiffness of the beam. Larger beams have experimental compliances very much closer to theoretical values than smaller beams. This is thought to be due mainly to the greater relative deformations experienced by the smaller beams resulting in greater crack-surface rotation and aggregate pull-out in the fracture zone; this in turn is thought to result in smaller crack-closing stresses.

6. Using the conventional compliance relation an "apparent" crack depth can be determined, which will generally be greater than the visible crack depth. Analysis of slow crack growth prior to maximum load shows that absolute values of apparent crack extension are greater in larger beams compared with smaller beams, however on a relative basis (i.e. crack growth/initial notch depth) the larger beams experience less slow crack

crack-closing stresses operate. Theoretical relationships that ignore this effect are therefore not entirely valid.

2. Using experimental load-deflection curve[illegible]s possible to define two compliances:- the conventional compliance which is simply the inverse slope of a line joining the origin to the point (F,δ) in question; and the modified compliance which is a reloading compliance obtained from the inverse of the slope of the linear portion of the reloading curve in any load cycle. The presence of the microcracked zone as well as irrecoverable deformation influences these compliances.

3. Initial notch compliances of the fracture beams agree well with theory. This is before any non-linearity and damage occurs.

4. Considerable irrecoverable deformation occurs, resulting from resistance to crack closing which is due to previous aggregate pull-out and crack surface disintegration.

5. Experimental compliance relationships based on visible crack growth show that the fracture beams are more compliant than theory would predict; this is to be expected due to the development of a microcracked zone which reduces the stiffness of the beam. Larger beams have experimental compliances very much closer to theoretical values than smaller beams. This is thought to be due mainly to the greater relative deformations experienced by the smaller beams resulting in greater crack-surface rotation and aggregate pull-out in the fracture zone; this in turn is thought to result in smaller crack-closing stresses.

6. Using the conventional compliance relation an "apparent" crack depth can be determined, which will generally be greater than the visible crack depth. Analysis of slow crack growth prior to maximum load shows that absolute values of apparent crack extension are greater in larger beams compared with smaller beams; however on a relative basis (i.e. crack growth/initial notch depth) the larger beams experience less slow crack

growth. Slow crack growth prior to maximum load is nevertheless appreciable even in large beams, and can amount to between 10 to 25 per cent of initial notch depth. It therefore cannot be ignored in fracture calculations. There appears to be a linear relationship between crack growth and initial residual ligament depth (h_0), crack growth reducing as h_0 increases. This should be useful for preliminary analysis of fracture parameters. However, for the notch-insensitive 100mm deep beams, it will be shown later that crack growth can be seriously overestimated using apparent values.

7 FRACTURE ZONE CHARACTERISATION USING STRAIN MEASUREMENTS

7.1 INTRODUCTION

Concrete fracture is complex due to the heterogeneous nature of the material. Cracking may comprise cleavage within the material leaving relatively stress-free crack surfaces. Alternatively cracking may be more incipient in that a zone of microcracking develops in those areas where tensile stresses are high, particularly due to stress concentrations. Such microcracked zones will be characterised by microscopic interface cracking between aggregate particles and matrix, and occasionally cracking within the matrix itself. Stress transfer across the microcracked zone will, in general, still be possible, and will reduce as the total displacement across the zone increases. These concepts have been introduced previously in 3.5.1 and figure 3.9; the intention of this chapter is to develop these concepts relative to fracture in beams, and to present experimental data on the measurement of fracture zones, using a strain gauge technique. The following chapter will present results of fracture zone measurements using an ultrasonic technique.

Four distinct stress zones may be identified in a notched fracture beam. With reference to figure 7.1 these are:-

1. A destressed zone characterised by a stress-free crack of depth c.

2. A microcracked zone, also called a fracture zone, which includes a zone of aggregate pull-out, and extends immediately ahead of the main crack tip. Tensile stress transfer may occur in this zone due to aggregate interlock and remaining matrix ligaments.

3. An intact tension zone, in which the material is essentially undamaged and stress-strain relationships are reasonably linear. The stress at the limit of this zone approaches the bulk tensile strength of the material.

4. A compression zone above the neutral axis in which the material is also essentially undamaged and stress-strain relationships are reasonably linear.

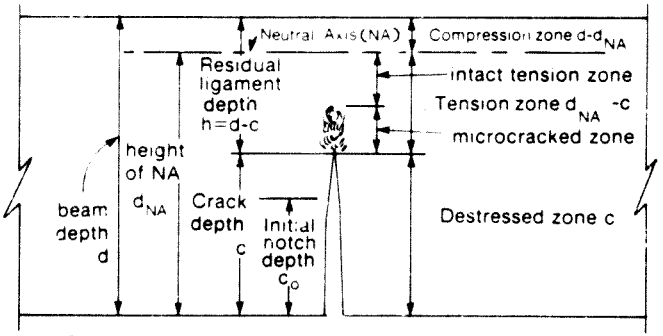

Figure 7.1 Definition of stress zones in a concrete beam during fracture

Figure 7.1 shows that the total tension zone comprises the microcracked zone and the intact tension zone. The residual ligament depth is defined as the difference between the beam depth d and the stress-free crack depth c. It is within the depth h that stress transfer of one form or another can occur.

In the present tests, neutral axis position was determined from strain profiles, and an estimate of the stress-free crack depth was obtained from the visible crack depth. It was desirable to try and

measure sizes of the microcracked zone, since generally up to now these have had to be inferred from theoretical models. An estimate of fracture zone size would also allow the material to be characterised relative to its fracture behaviour.

"Demec" strain targets at mid-span and covering the beam height were fixed to one side of all beams of series F3 on a 100mm gauge length. Details of the mechanical gauges and their positions have been given in 4.4.3. Strains were generally read as close to the peak of each load cycle as possible. Data involved four strain readings, mid-span load and deflection, and visible crack depth for each cycle. Strain or displacement profiles across the mid-span section could then be plotted. Strain readings were converted to displacements within the crack once the crack had intersected the relevant strain measuring position. This allowed crack widths and crack opening displacements (COD) at crack tips to be measured.

This section is concerned with presenting the strain and crack displacement results, and interpreting these results in terms of the effect of notches on beams, crack opening displacements at crack tips, the relation between compression and tension zones in a beam during fracture, development of microcracked zones, and use of strain profiles to assess zone sizes.

7.2 STRAIN AND DISPLACEMENT PROFILES

The development of very large tensile strains during the early stages of loading indicated that microcracking and actual crack advance occurred early on. Visible crack advance was usually positively identified during the maximum load cycle, and cycles immediately thereafter resulted in substantial crack advance. Therefore the majority of the strain readings for the maximum load and subsequent cycles had to be interpreted as displacements across crack faces. Displacements were found by multiplying "strain" values by gauge length and expressing the results in micron units

(i.e. m x 10^{-6} = μm). For the sake of consistency in the diagrams, the strains in the "intact" portions of the beam were also expressed as equivalent displacements across the gauge length (For the 100mm strain gauge used in the majority of the readings, 1μm of displacement represented 10 microstrain units).

Typical displacement profiles for the range of beam sizes of series F3 are shown in figures 7.2, 7.3, 7.6 and 7.7. Results for beams with initial notch-depths of 0,2 or 0,4 were very similar. Profiles for the *maximum load* and *subsequent cycles* are shown. A number of interesting points emerge from the figures, as follows:-

FIGURE 7.2 (F3/1 (500/0,2))

1. The profile for the lower part of the beam is remarkably linear at all stages. The linearity of the overall profile improves as the test progresses. In early cycles there is a marked discontinuity in the profile.

2. The values of COD at the visible crack tip were found by drawing a horizontal line from the position of the visible crack tip to intersect the relevant profile line. These values varied from 57μm to 72μm for this beam (see insert table in figure 7.2). The overall variation including results from other 500mm beams was 38μm to 94μm, with the 0,4 notch-depth beams generally showing smaller values. The variation in COD values indicates that the exact position of the crack tip was not always easy to determine visually. However, for any one beam, the range of COD values was fairly limited, indicating consistency during a single test. The most probable reason for the deeper notched beams giving smaller COD values is that the deeper notch generated a more distinct crack. The insert table shows that COD values for this beam reduced as the crack grew during the test, although this was not always evident in all the beams.

It was noted on occasions that when strain readings at a particular position were well in excess of 100.10^{-6}, the visible crack tip had not yet intersected this position. Concrete in tension can be expected to crack when the strain reaches approximately 100.10^{-6}, and the deduction is that microcracking occurred in these cases but was not clearly visible to the naked eye. These strain readings were therefore interpreted as opening displacements.

3. There is a rapid rise in the neutral axis (N.A.) position during the test (see inset table). Even at the peak load cycle (cycle 2) the N.A. has moved well up in the beam, indicating the development of an extensive microcracked tension zone.

4. Maximum crack mouth displacements (CMD) that were measured during the last cycle before final fracture varied from about 1,2mm to 1,9mm, for 500mm beams. These values were measured at position 1.

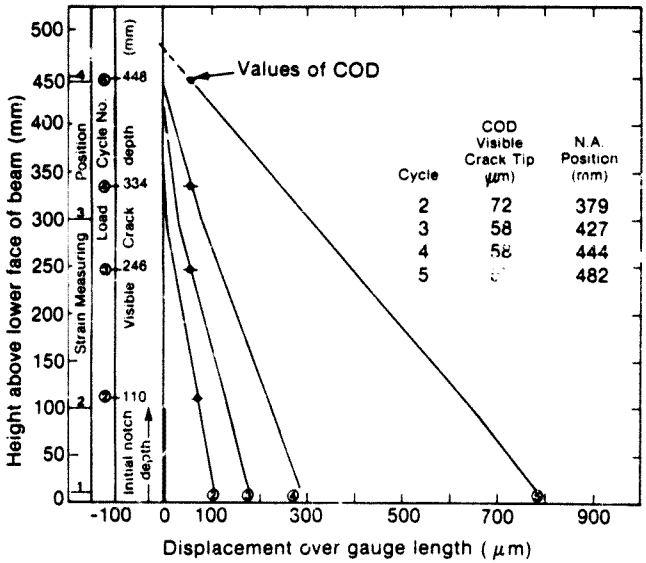

Figure 7.2 Displacement profile for beam F3/1(500/0,2)

FIGURE 7.3 (F3/6 (300/0,2))

1. The linear profile in later loading cycles is very evident in this figure. The maximum load cycle (cycle 2) has a distinct discontinuity in the profile. Comparison of the profile for cycle 4 in this figure with that for cycle 4 in figure 7.2 shows that, for a similar ratio of CMD to beam depth, the 300mm deep beam appears to have a more linear profile. A similar trend may be noticed by comparing profiles for cycles 2 (300mm beam) and 3 (500mm beam).

2. The neutral axis position shifts up very rapidly, and then more or less stabilises as the residual ligament depth h becomes small. Between cycles 4 and 5 there is nominally no change in neutral axis position, and this is mirrored by the small change in visible crack depth. It can be concluded that the neutral axis experiences rapid change in position in the early stages of loading, with rapid increase in crack depth and development of a microcracked zone; at this stage there is only limited increase in crack width. In later stages of loading, the crack depth and neutral axis position change slowly, but the crack width begins to increase enormously.

The relationship between crack depth and crack width is shown in figure 7.4, where crack width is expressed as values of CMD divided by the load at the relevant cycle. (Division by the load ensures that the points from the various beams can be compared). Initially a microcracked zone develops with increase in CMD but no increase in c. This is true for both init[illegible] h depth ratios shown in the figure. Thereafter a per[illegible] crack growth occurs, while crack width increases st[illegible] well. When crack depth exceeds about 60 per cent of beam [illegible], the rate of increase in CMD/F becomes very large so that ultimately for very little crack growth there is an enormous increase in crack width. This effect

of increase in crack width without significant crack growth was frequently observed during the tests.

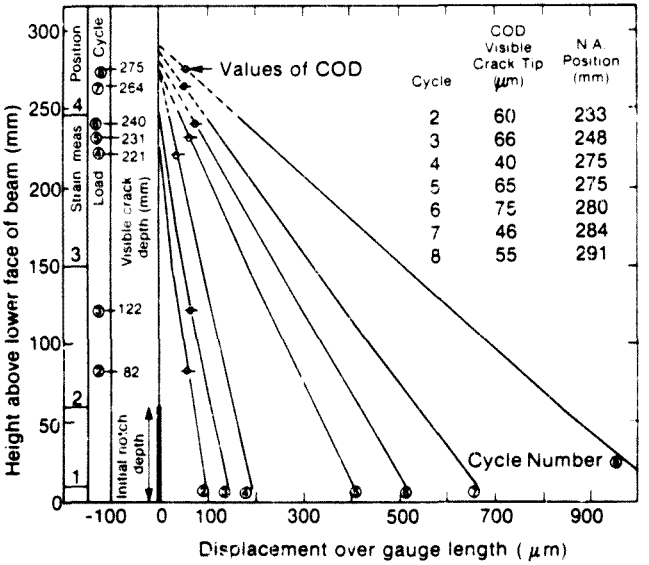

Figure 7.3 Displacement profile for beam F3/6(300/0,2)

Other interesting features to note from figure 7.4 are that curves for the two initial notch depth ratios merge within the steady crack growth region and follow a single curve for any particular beam size. Initial notch depth therefore affects only the development of the initial microcracked zone in respect of its size, but later cracking is unaffected by initial notch depth. Within the steady crack growth region there is a differentiation between curves for different beams, smaller beams showing larger CMD/F values. This is consistent with the argument in 6.6.3 and figure 6.7 where it was shown that smaller beams experienced greater crack-face rotations from a consideration of irrecoverable deformations. If typical values of load F are taken for 100mm and 500mm beams at a given c/d value it can be shown from figure 7.4 that crack rotations

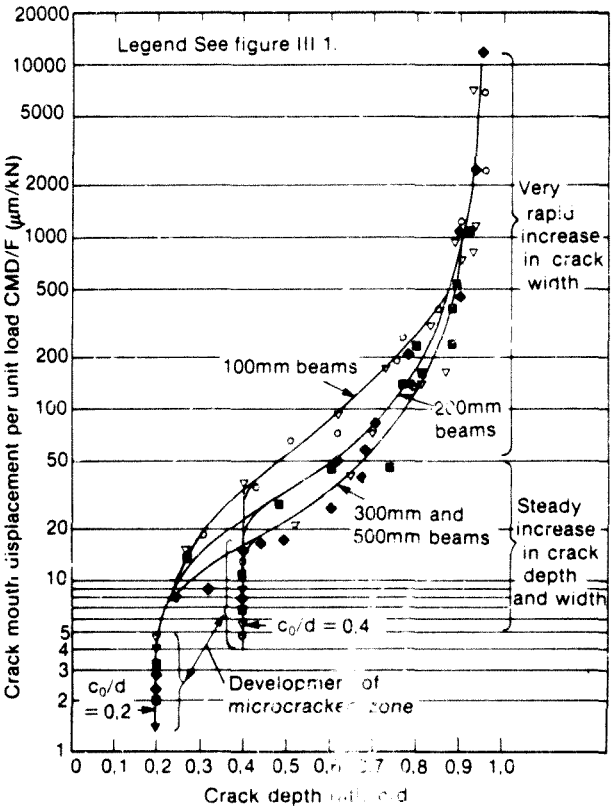

Figure 7.4 Relationship between crack depth and crack mouth displacement

in 500mm beams will be between two to three times as great as those in 100mm beams, which agrees with the figure of 2,5 given in 6.6.3.

The mean lines in figure 7.4 have been replotted in natural scale in figure 7.5.to produce compliance curves, which mirror the curves in figures 6.5 and 6.8. It appears that compliance measurements based on CMD give a smaller separation between mean curves for different beam sizes than compliance based on deflection.

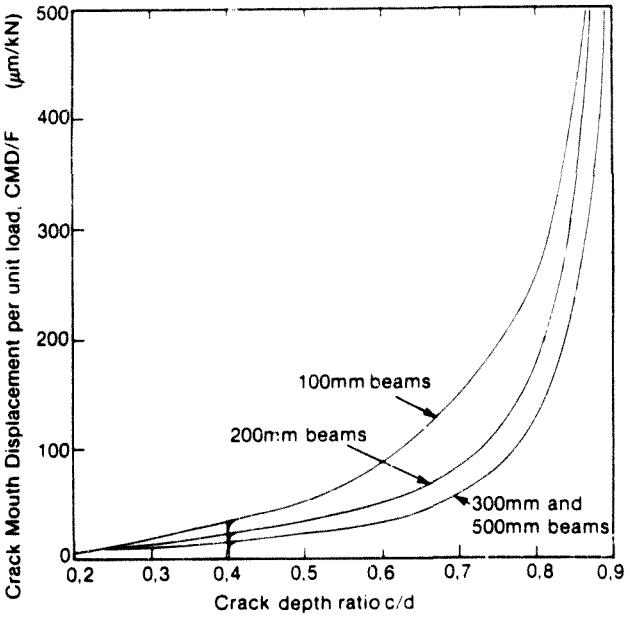

Figure 7.5 Crack mouth displacement compliance curve obtained from figure 7.4

FIGURE 7.6 (F3/13 (200/0,2))

1. Cycles immediately following maximum load have virtually linear profiles.

2. COD values vary from 15μm to 50μm, with values decreasing higher in the beam. Since gauge position 4 was approximately at the neutral axis position for later load cycles, any inaccuracy in strain readings at this point would critically affect the COD values. The proximity of this gauge position to the neutral axis also resulted in difficulty in defining the profile above this point. For instance, cycle 5 shows a COD value of 0, whereas in reality the profile should steepen beyond this gauge postion in order to accommodate a tension and compression zone in the remaining "intact" region of the beam.

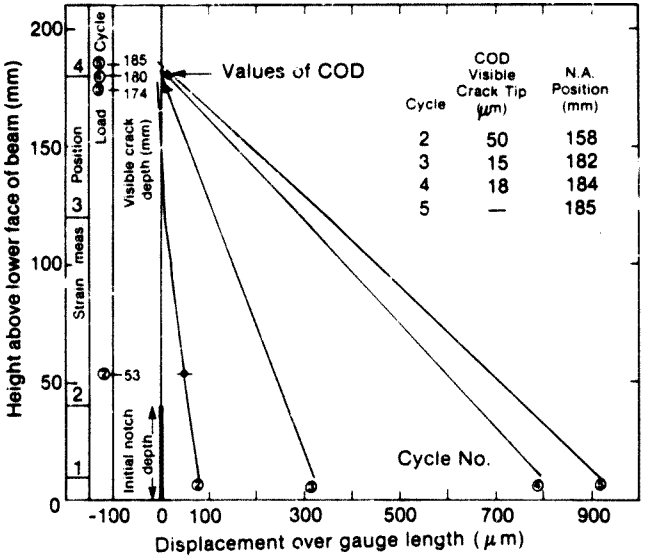

Figure 7.6 Displacement profile for beam F3/13(200/0,2)

FIGURE 7.7 (F3 19 (100/0,2))

1. Linear profiles beyond maximum load cycle are again apparent. COD values at crack tips are similar to those for 200mm beams.

2. The problem of gauge position being at the neutral axis position mentioned for the 200mm beams is accentuated here. Cycle 5 has a crack depth above the nominal neutral axis position which must indicate that the strain profile changes in the upper intact portion of the beam, becoming considerably steeper and shifting the neutral axis further up. Assuming a critical COD at the visible crack tip of between 10 to 20 μm, the likely extension to the profile for cycle 5 has been drawn on the diagram.

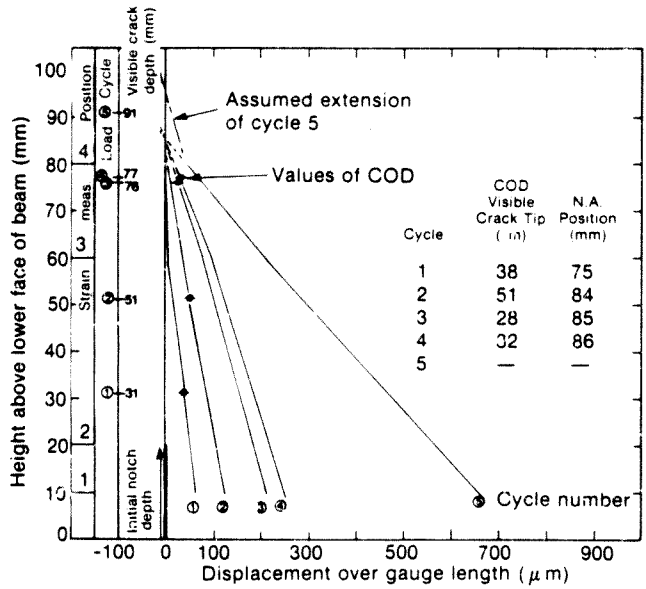

Figure 7.7 Displacement profile for beam F3/19(100/0,2)

7.3 COMPARISON OF COD VALUES

A crucial question in assessing crack depths and COD values is that of determining the point at which crack faces are truly stress-free. This will be a function of a critical COD value, and the question also arises whether such a value varies with beam depth. The COD values at visible crack tips were analysed for three 500mm beams, four 300mm beams, three 200mm beams, and three 100mm beams of series F3. The results are shown in figure 7.8. A large spread of results has occurred, but there is a clear trend of COD increasing with increasing beam depth.

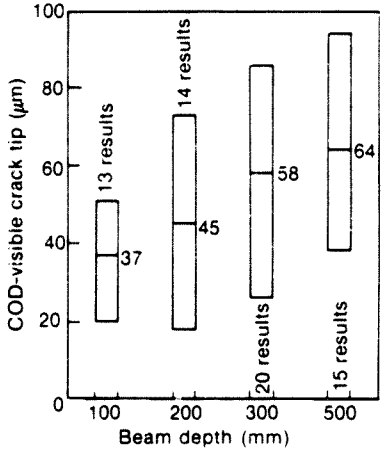

Figure 7.8 Mean values and spread of results for COD at visible crack tip (series F3)

The values in figure 7.8 are interesting when compared with analytical values or critical COD at the limit of a stress-free crack suggested by Wecharatana and Shah[69]. They deduced a value of about 25μm for concrete which is somewhat smaller than the present values. The initial residual ligament length of Wecharatana and Shah's double cantilever beams was about 500mm, making them comparable

with the large beams of series F3. They quote results of COD for a polymer material (PMMA) as being between 2 to 3 μm. Thus, the COD will depend on the particular material being tested. Wecharatana and Shah applied their critical value of 25μm to estimate microcracked zone size by a theoretical analysis of the work of other investigators. Applying this value as the critical limit of a stress-free crack (and hence the limit of the tension zone) to, say, cycle 4 of beam F3/6 (figure 7.3), we get a crack depth of 242mm (as opposed to observed visible crack depth of 221mm). The following analysis then applies:-

Crack depth = 221mm *N.A. height = 275mm*
Compression zone = 300-275 = 25mm
Tension zone = 275-221 = 54mm

The compression zone is smaller than the tension zone because in the tension zone, and in the microcracked zone in particular, the stresses are decaying and a longer tension zone is required for internal force equilibrium.

From later section 7.6, an estimate of microcracked zone size for h = 300-221mm (i.e. 79mm) would be 37mm. Therefore the "intact" tension zone is 54-37mm = 17mm. This value appears reasonable relative to compression zone size of 25mm.

Crack depth = 242mm *N.A. height = 275mm*
Compression zone = 300-275 = 25mm (as above)
Tension zone = 275-242 = 33mm.

Assuming the microcracked zone size is now about 27mm (from section 7.6 with h = 58mm), the "intact" tension zone is 33-27 = 6mm. This value is unrealistic relative to compression zone size.

The above argument indicates, at this stage at least, that estimated COD values at the tips of stress-free cracks are critical in obtaining correct solutions.

with the large beams of series F3. They quote results of COD for a polymer material (PMMA) as being between 2 to 3 μm. Thus, the COD will depend on the particular material being tested. Wecharatana and Shah applied their critical value of 25μm to estimate microcracked zone size by a theoretical analysis of the work of other investigators. Applying this value as the critical limit of a stress-free crack (and hence the limit of the tension zone) to, say, cycle 4 of beam F3/6 (figure 7.3), we get a crack depth of 242mm (as opposed to observed visible crack depth of 221mm). The following analysis then applies:-

Crack depth = 221mm N.A. height = 275mm
Compression zone = 300-275 = 25mm
Tension zone = 275-221 = 54mm

The compression zone is smaller than the tension zone because in the tension zone, and in the microcracked zone in particular, the stresses are decaying and a longer tension zone is required for internal force equilibrium.

From later section 7.6, an estimate of microcracked zone size for h = 300-221mm (i.e. 79mm) would be 37mm. Therefore the "intact" tension zone is 54-37mm = 17mm. This value appears reasonable relative to compression zone size of 25mm.

Crack depth = 242mm N.A. height = 275mm
Compression zone = 300-275 = 25mm (as above)
Tension zone = 275-242 = 33mm.

Assuming the microcracked zone size is now about 27mm (from section 7.6 with h = 58mm), the "intact" tension zone is 33-27 = 6mm. This value is unrealistic relative to compression zone size.

The above argument indicates, at this stage at least, that estimated COD values at the tips of stress-free cracks are critical in obtaining correct solutions.

7.4 EFFECTIVE STIFFNESS OF FRACTURE ZONES

The displacement profiles described above have indicated that in a notched and fracturing cross-section, plane sections do not remain plane, particularly during the early stages of loading when the main crack is extending rapidly. At later loading stages, the linearity of the profile is again re-established. The progress of cracking may be described as follows:-

1. At onset of loading when loads are small, the section remains plane and acts essentially as an ordinary beam with a flexural rigidity corresponding to the notched cross-section. This condition is maintained until stresses at the notch root approach the tensile strength of the material.

2. As load is increased, the notch begins to exercise a dominating influence on the tension zone, with the very rapid development of a microcracked non-linear zone ahead of the notch. Once this microcracked zone reaches a limiting (maximum) value, the main crack begins to extend causing the microcracked zone to further extend.

3. The effect of the microcracked zone is to create a "centre of rotation" or point of discontinuity in the beam. Above the zone, the material is "intact" and retains its normal stiffness, while the zone extending behind the main crack tip is effectively destressed. In the microcracked zone itself, the material is suffering "damage" by the effect of the stress concentration, and therefore the effective stiffness of the zone decreases[11].

4. As the main crack extends higher in the beam, the microcracked zone reduces in size, and its effect as a centre of rotation also reduces. Ultimately when the crack closely approaches the upper face, the stress concentration effect is lost and the remaining "intact" portion of the beam acts once again according to classical beam theory, with a normal material stiffness.

(Note that the possibility of the strain profiles being distorted due to a deep beam (shear) effect for the present beams has been excluded on the grounds that a deep beam is normally defined as one with span/depth ≤ 2 (see for example the recommendations of CEB-FIP (1970)[88]). The present profiles with two distinct linear regions also differ from a normal shear-distorted profile which would be markedly non-linear).

It was noticed from the displacement profiles that shallower beams seemed to suffer less from the distortional effect than deeper beams. This was presumably because shallower beams were less notch-sensitive, which, interpreted in the light of displacement profiles, implies that the notch had a less marked effect in producing non-planar sections. To test this hypothesis, use was made of simple classical beam theory applied to the strain profiles measured in the tests. The theory states that the slope of the strain profile is proportional to curvature, and hence to applied moment divided by flexural rigidity. It was possible to measure slopes of strain profiles, and infer an effective stiffness of the fractured zone. The development of the method is given below.

From classical beam theory,

$$\frac{M}{EI} = \frac{\sigma}{Ey} = \frac{\varepsilon}{y} \qquad (7.1)$$

where M is the applied moment, EI is the flexural rigidity (E and I having their normal meanings) and ε/y is the slope of the strain profile. For the present beams, $M = FS/4$, where F is the mid-span applied load, and S is support span. Therefore we can write:-

$$\frac{FS}{4EI} = \frac{\varepsilon}{y} \qquad (7.2)$$

Re-arranging, we get:-

$$\frac{1}{F}\frac{\varepsilon}{y} = \frac{S}{4EI} \qquad (7.3)$$

Since S = 4d for the beams, and using an I value equivalent to the cracked section, we get:-

$$\frac{1}{F}\frac{\varepsilon}{y} = \frac{4d}{4E}\,\frac{1}{(bh^3/12)} \qquad (7.4)$$

where h = d - c.
This finally reduces to

$$\frac{1}{F}\frac{\varepsilon}{y} = \frac{2}{EZ}\left(\frac{d}{h}\right)^2 \qquad (7.5)$$

where Z = the full section modulus ($bd^2/6$).

The only unknown in equation (7.5) is the elastic modulus or stiffness of the material. This can be evaluated since all other terms can be calculated from the experimental record. The resulting E value is termed the "effective stiffness", E_{eff}.

The profiles in figures 7.2, 7.3, 7.6 and 7.7 indicate that the effective stiffness found from equation (7.5) will vary in the depth of the beam, particularly for profiles from earlier stages of loading. For later loading cycles, the profiles become virtually linear. The degree of non-linearity of a profile can therefore be assessed by comparing the slope of, say, the lowest section with the overall mean slope. For a perfectly linearly elastic material the overall profile slope will be uniform and represent the stiffness E of the material. It is therefore convenient to express the slopes referred to above as ratios of E_{eff} to the measured E values for the beams (see table 5.4). We can thus plot ratios of E_{eff}/E for the lowest portion of the profile and for the profile as a whole, against crack depth ratio c/d. The differences between the two curves can be taken to indicate the magnitude of planar distortion.

Figures 7.9(a) to (d) show the effective stiffness plots for the four beam sizes of series F3. (Each figure was produced by plotting the results for three beams of any one size, except the curve for the 100mm beams. See later comment). The E_{eff} reduces rapidly on initial loading, before any visible crack growth occurs. This is shown by the vertical lines at c/d = 0,2. Thereafter, the E ratio reaches a minimum with a relatively small degree of crack growth, and then increases with further crack growth. The curve for the overall profile (curve 'A') lies above the curve for the lowest portion of the profile (curve 'B') as expected. The following points should be noted:-

1. The results for the 100mm beams had a very wide scatter and it was thought best to plot results for two beams representing extreme cases (i.e. F3/17 and F3/19, both 100/0,2). In the first case, it can be seen that crack growth actually occurred to a c/d value of about 0,3 before E_{eff} reduced. Thereafter the reduction in E_{eff} was small, and with increasing crack growth the E ratio approached unity again at c/d = 0,7. There was essentially no difference between the overall strain profile slope and the slope of the lowest portion, i.e. the section remained plane. In the second case, E_{eff} reduction was larger. Curve 'A' lay slightly above curve 'B', but over a relatively short period of crack growth. The maximum vertical separation between the two curves was limited. This indicated that the profile did not deviate much from linearity.

2. Mean "trend" curves for the 200mm beams were plotted; these curves are very similar to the curves for F3/19 discussed above. However, the minimum value of the E ratio was substantially lower than for the 100mm beams. This indicated that the crack had a more severe effect in reducing the effective material stiffness (i.e. the distortion of the plane section was more severe). The maximum separation between curves 'A' and 'B' was slightly greater than for F3/19, indicating a greater degree of non-linearity; this effect also occurred over only limited crack growth.

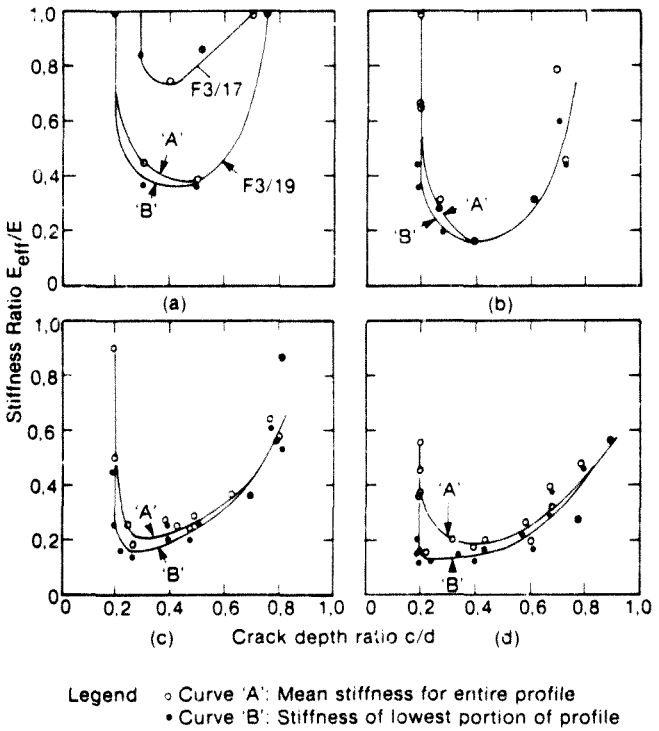

Figure 7.9 Effective stiffness curves for (a) 100mm beams (b) 200mm beams (c) 300mm beams (d) 500mm beams (series F3)

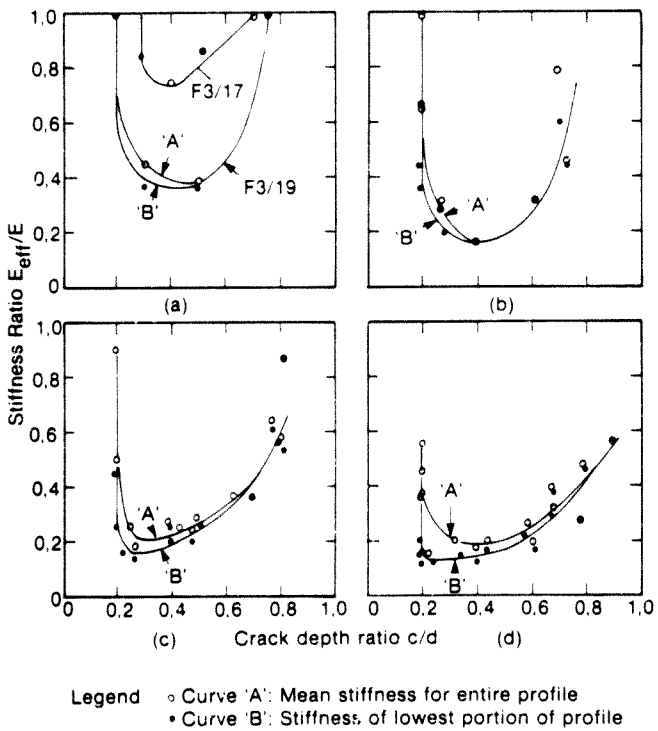

Figure 7.9 Effective stiffness curves for (a) 100mm beams (b) 200mm beams (c) 300mm beams (d) 500mm beams (series F3)

3. The curves for the 300mm beams indicate that on first loading there was an immediate reduction in E_{eff} for the lower portion of the beam, and the degree of non-linearity of the strain profile was greater than for the shallower beams. The distortional effect was very marked for these beams, as witnessed by the total E_{eff} reduction and the maximum separation between curves 'A' and 'B'. This effect persisted over a greater portion of crack growth than for the shallower beams. These remarks also hold true for the 500mm beams, although to an even greater degree. In these beams, planar distortion achieves its greatest effect which is also sustained for the longest portion of crack growth.

The curves in figure 7.9 illustrate the marked difference in fracture behaviour between various beam sizes. They also confirm the notch-sensitivity curves in figure 5.6. In smaller beams, development of a microcracked zone is restricted by overall depth limitation, and plane sections are very little distorted during fracture. The overall beam stiffness will reduce but not to the same degree as for deeper beams, and as cracking progresses the stiffness quickly approaches its conventional value again. In essence, the notch has a very limited effect, and the specimen is not really notch-sensitive. Conversely, for deeper sections a marked non-linear strain profile occurs which is sustained for the major portion of crack growth. The effect of the notch is to severely reduce effective beam stiffness below the neutral axis, thus indicating a large rotational distortion. These beams are therefore notch-sensitive. The trends in figure 7.9 confirm that notch-sensitivity increases with increasing beam depth.

7.5 COMPRESSION AND TENSION ZONES IN BEAMS DURING FRACTURE

In order properly to analyse fracture in a notched beam, it is necessary to know the extent of the compression and tension zones.

During fracture, linear stress distributions no longer apply due to the dominant influence of the notch or crack (provided the material is, of course, notch-sensitive). For cemented materials in particular, the zone below the neutral axis will consist of three regions, which have been discussed in 7.1. In the microcracked region the concept of average strain begins to break down, and deformation is more in the form of displacements arising from crack cleavage. The de-stressed region behind the main crack tip will consist of material damaged by the process of crack growth. For plain concrete, a fracturing beam will have tension and compression zones that will not be equal in depth due to the limited ability of the concrete to carry tensile stresses. In other words, for internal equilibrium of forces, the tension zone must be deeper than the compression zone. In this section the results of the strain measurements are analysed to obtain a characteristic relation between tension and compression zone sizes for the beams of series F3.

Referring to figure 7.1, the compression and tension zone depths are described by the following simple equations:-

$$\text{Compression zone depth} = d - d_{NA} \qquad (7.6)$$

$$\text{Tension zone depth} = d_{NA} - c \qquad (7.7)$$

where d_{NA} is the height of the neutral axis above the lower face of the beam. The de-stressed zone of length c behind the main crack is therefore not included in the tension zone.

The measuring of strains in the beam cross-section has allowed confident determination of d_{NA}. The relation between compression and tension zone depths, with c as the measured visible crack depth, could therefore be plotted. This has been done in figure 7.10 using the results of thirteen beams from series F3 (three x 500mm, four x 300mm, three x 200mm, and three x 100mm beams). Two characteristic straight lines have been plotted on the figure:- a 45° line representing an equal compression and tension zone size and a line giving the experimental relationship for the beams. This line has

an equation obtained by linear regression of the fifty experimental points (and which has been constrained to pass through the origin) as follows:-

$$(d-d_{NA}) = 0,461(d_{NA}-c) \qquad (7.8)$$

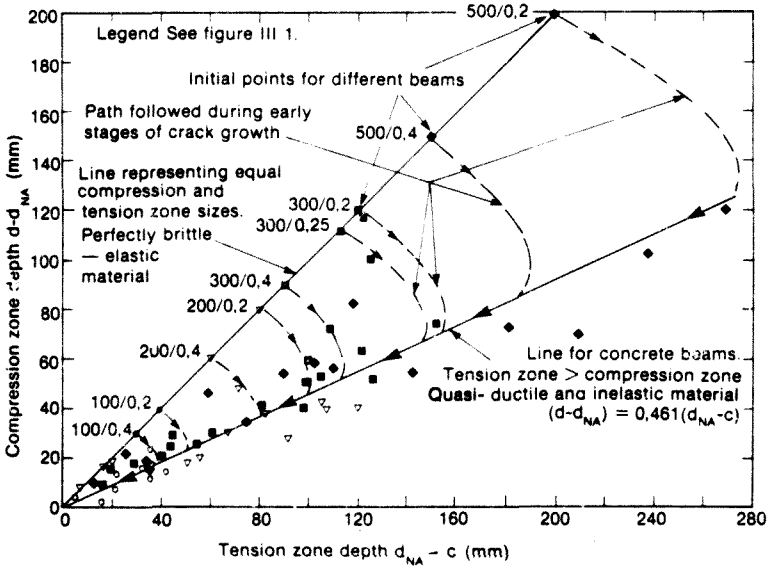

Figure 7.10 Relationship between compression and tension zone depths in concrete beams during fracture

Note the following from figure 7.10:-

1. Results from all beam sizes fall essentially along one straight line - the characteristic line for the particular concrete beams tested. The fracture process follows a similar course for all beams.

2. On initial loading, experimental points actually fall on the 45° line indicating that, before any damage or crack extension has occurred, the classical condition of equal compression and tension zones applies. The initial points for the different beam types can be seen on the 45° line.

3. During early stages of loading, there is rapid development of the tension zone at the expense of the compression zone, shown by the dashed lines of negative slope which eventually curve around to meet the characteristic line at different points depending on beam size. This path is followed as a zone of microcracking is developed and due to initial crack advance which forces the neutral axis up in the beam. It was not always possible to obtain experimental points along dashed lines, and these should therefore be regarded as trend lines.

4. The full development of the microcracked zone occurs at the points of tangency of the curved dashed lines with the characteristic line. During intermediate and later stages of loading, beam behaviour follows the characteristic line backwards towards the origin. The relationship between tension and compression zone sizes remains constant during crack growth. The zones are therefore reducing in size, but at a constant ratio. According to equation (7.8), this ratio is 1/0,461 = 2,17, indicating that the size of the tension zone is slightly more than twice that of the compression zone.

7.5.1 MATERIAL CHARACTERISATION FROM TENSION/COMPRESSION ZONE SIZE RELATION

The characteristic straight lines in figure 7.10 represent specific types of material behaviour. The 45° line represents an ideal elastic-brittle material, since fracture occurs at some limiting tensile stress without development of a microcracked zone and the stress distribution is linear, i.e. the compression and tension

zone sizes are equal throughout the fracturing process. The characteristic line for the concrete beams is well removed from the "ideal" brittle material line, indicating a material that is quasi-ductile due to the presence of a microcracking zone which prevents truly brittle behaviour from occurring. There is also considerable non-linearity in strain and stress profiles. It may therefore be postulated that the further the characteristic lin of a material falls below the 45° line, the less idea elastic-brittle is the material. The converse is also true; therefore a material like hardened cement paste can be expected to have a line falling very much closer to the 45° line than the concrete line, with mortar falling between the paste and concrete lines. The line representing the simple relationship between compression and tension zone sizes in a beam during fracture may therefore be regarded as characteristic of material fracture behaviour.

7.5.2 POSITION OF BEAM NEUTRAL AXIS DURING FRACTURE

Equation (7.8) was derived from the experimental relation between compression and tension zone sizes in fracturing beams. The sizes of these zones depend upon the neutral axis position, and it is possible to obtain a relationship between neutral axis position and some other convenient geometrical parameter of the beam; the most convenient parameter is the residual ligament depth h (= d-c), which allows comparison between results of different beams.

From equation (7.8), we can develop the following:-

$$d-d_{NA} = 0,461\ (d_{NA}-c)$$

or

$$(d-c)-(d_{NA}-c) = 0,461\ (d_{NA}-c)$$

Therefore:-

$$(d_{NA}-c)(1,461) = (d-c)$$

Finally:-

$$d_{NA}-c = \frac{(d-c)}{1,461}$$

$$= 0,684\ (d-c) \qquad (7.9)$$

This relationship has been plotted in figure 7.11, together with fifty-one experimental points from the thirteen beams of series F3 mentioned earlier. Equation (7.9) is effectively the linear regression equation between $(d_{NA}-c)$ and $(d-c)$ since the governing equation (7.8) was obtained by linear regression. It should be pointed out that figure 7.11 represents conditions in a beam *during fracture* i.e. while crack growth is in progress. A dashed line is drawn in figure 7.11, representing neutral axis position in an ideal elastic-brittle material. This position is the lower limit that can be adopted by the neutral axis, and represents equal compression and tension zone sizes. In the case of figure 7.11, the higher the experimental line falls above the theoretical lower limit line, the more removed the material is from the simple "ideal" case.

It is possible to re-arrange equation (7.9) to express the neutral axis position directly as:-

$$d_{NA} = 0,684\ d + 0,316c \qquad (7.10)$$

This predicts that in an unnotched beam (c=0) at the point of incipient fracture, the neutral axis should lie roughly two-thirds of the way up the height of the beam. In fact the neutral axis will lie at a position above the crack tip roughly two-thirds of the distance between the crack tip and upper face of the beam.

The striking aspects of figure 7.11 are the small scatter of results and the fact that experimental points from beams with overall depths from 100mm to 500mm all lie along one straight line. The correlation coefficient for the linear regression line has a value of 0,996 indicating very strong correlation and an excellent fit of experimental results. However, it should be noted that for h less than about 50mm, the results tend to lie more along the lower limit line, indicating that for these very shallow beams the zone of microcracking is extremely small and does not influence the re-

$$d_{NA}-c = \frac{(d-c)}{1,461}$$

$$= 0,684\ (d-c) \qquad (7.9)$$

This relationship has been plotted in figure 7.11, together with fifty-one experimental points from the thirteen beams of series F3 mentioned earlier. Equation (7.9) is effectively the linear regression equation between $(d_{NA}-c)$ and $(d-c)$ since the governing equation (7.8) was obtained by linear regression. It should be pointed out that figure 7.11 represents conditions in a beam *during fracture* i.e. while crack growth is in progress. A dashed line is drawn in figure 7.11, representing neutral axis position in an ideal elastic-brittle material. This position is the lower limit that can be adopted by the neutral axis, and represents equal compression and tension zone sizes. In the case of figure 7.11, the higher the experimental line falls above the theoretical lower limit line, the more removed the material is from the simple "ideal" case.

It is possible to re-arrange equation (7.9) to express the neutral axis position directly as:-

$$d_{NA} = 0,684\ d + 0,316c \qquad (7.10)$$

This predicts that in an unnotched beam (c=0) at the point of incipient fracture, the neutral axis should lie roughly two-thirds of the way up the height of the beam. In fact the neutral axis will lie at a position above the crack tip roughly two-thirds of the distance between the crack tip and upper face of the beam.

The striking aspects of figure 7.11 are the small scatter of results and the fact that experimental points from beams with overall depths from 100mm to 500mm all lie along one straight line. The correlation coefficient for the linear regression line has a value of 0,996 indicating very strong correlation and an excellent fit of experimental results. However, it should be noted that for h less than about 50mm, the results tend to lie more along the lower limit line, indicating that for these very shallow beams the zone of microcracking is extremely small and does not influence the re-

sults. This is again tantamount to saying that, for the present material, such beams will be notch-insensitive due primarily to the restraint of overall size.

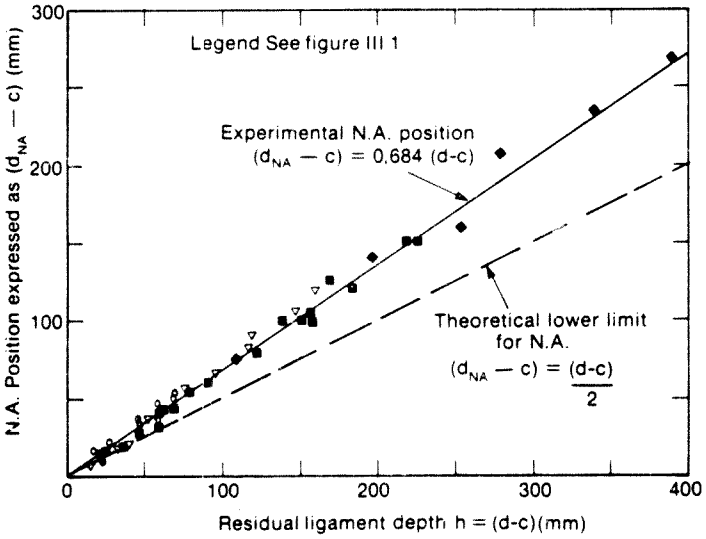

Figure 7.11 Dependence of neutral axis position on residual ligament depth in beams during fracture

7.5.3 LIMITS TO SIZE OF MICROCRACKED ZONE

The experimental relationship between compression and tension zone sizes (equation 7.8) can be used to obtain lower and upper limits for the size of the microcracked zone in a beam during fracture. Given the definition of zone sizes in figure 7.1, the main concept to be borne in mind is the assumption that some degree of stress transfer occurs within the microcracked zone, which is the reason for its inclusion within the tension zone. Considering cemented

materials such as concrete, the following argument can be advanced to develop an expression for a lower limit to the microcracked zone size in a fracturing beam:-

1. During initial stages of loading, the neutral axis remains halfway between the notch root and the extreme fibre of the compression zone. As soon as tensile stress at the notch root exceeds tensile strength, the neutral axis shifts rapidly upwards and a zone of microcracking develops. This process occurs under increasing load. Since the intact tension zone can carry only limited maximum stress the microcracked zone is required to provide an overall additional tensile force for moment equilibrium.

2. The greater the ability of the intact tension zone to carry tensile stress, the less additional tension is required from the microcracked zone. Assuming that the microcracked zone, due to its state of damage, can effect only limited stress transfer, then the size of this zone will reduce as the intact tension zone carries more stress. Conversely, for an intact tension zone that can effect only a limited maximum stress transfer, the microcracked zone will exhibit its smallest depth when the intact tension zone is carrying its maximum stress. For cemented materials, this occurs when the value of the stress at the limit of the intact tension zone equals the tensile strength.

3. The limiting condition for cemented materials will occur when the force in the intact tension zone balances the force in the compression zone. The microcracked zone then no longer carries any stress, and will be at its minimum size.In the limit the microcracked zone can therefore be regarded as a direct extension of the stress-free crack.

The above argument implies that the lower limiting size for the microcracked zone (mcz) will equal the total tension zone depth minus the compression zone depth. Referring to figure 7.1:-

$$\text{Lower limit to mcz} = (d_{NA}-c)-(d-d_{NA}) \qquad (7.11)$$

Substituting for $(d-d_{NA})$ from equation (7.8) and for $(d_{NA}-c)$ from equation (7.9), this reduces to:-

$$\begin{aligned}\text{Lower limit to mcz} &= 0{,}684(d-c)-0{,}461\ (0{,}684)(d-c)\\ &= 0{,}368(d-c)\\ &= 0{,}368\ h \qquad (7.12)\end{aligned}$$

An upper limit to the microcracked zone size can be found from the fact that this zone cannot extend above the N.A. position. In this limiting case, the microcracked zone comprises the entire tension zone. Practically, this would require strain profiles with extreme slopes which are unlikely to occur in plain concrete. Thus we can write the following, from equation (7.9):-

$$\text{Upper limit to mcz} = 0{,}684\ (d-c) \qquad (7.13)$$

Equations (7.12) and (7.13) provide a framework within which experimental results or theoretical calculations of the microcracked zone size can be evaluated. Figure 7.12 shows the two limits plotted as functions of residual ligament depth. Note that the lower limit gives the condition in which the microcracked zone has zero stress transfer, and the upper limit the condition in which the microcracked zone contributes the tension component entirely. Therefore the positions that experimental results or other predictions occupy relative to these limits will indicate roughly the degree of stress transfer in the microcracked zone. In this sense the experimental lines are again characteristic of the particular material; for instance fibre reinforced materials with considerable stress transfer can be expected to have results which lie close to the upper limit, while hardened cement paste will have a characteristic line close to or coincident with the lower limit. (The question of limits to microcracked zone size will be further examined in chapter 9 relative to stresses in fracture zones. It will be shown there that, in fact, it is impossible for normal cemented

materials to achieve the upper limit condition described in equation (7.13)).

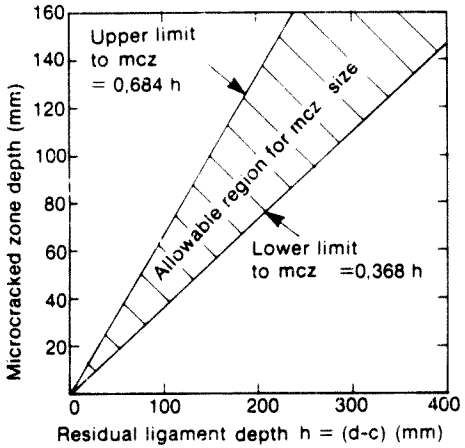

Figure 7.12 Limits to microcracked zone size as functions of residual ligament depth

7.6 MICROCRACKED ZONE SIZE DETERMINED FROM DISTORTION OF STRAIN PROFILES

The strain (or displacement) profiles discussed above have introduced the concept of distortion of plane sections occurring within a fracturing cross-section. The strain profile consists of two sections with differing slopes. The two slopes are separated by a point of discontinuity which exists because of development of a zone of microcracking ahead of the main crack tip, and within which the material is suffering damage. The microcracked zone is bounded at one end by the stress-free crack tip and at the other by the transition from "damaged" to "intact" material. Depending on the state of internal damage, the material will exhibit a characteristic

stiffness; this will vary from the normal stiffness of intact material to very much reduced stiffness of fully microcracked material. Within the microcracked zone, the stiffness is being continually lowered as the microcracking extends, until a limiting lower value is reached. This is generally when the zone has reached its fullest extent at any particular point in the section. Considering such a point which has become fully microcracked, further advance of the main crack will cause the point to lie behind the point of discontinuity and exhibit low stiffness.

The above description of the cracking process suggests that two distinct stiffnesses can be identified in a fracturing section:- a high stiffness of intact material, and a low stiffness of damaged material. Separating these two extremes is the zone in which microcracking is occurring. It should therefore be possible to identify the limit of the microcracked zone in a cross-section by measuring strains, drawing strain profiles in the section, and then defining the point of discontinuity. This point will be the intersection between two lines with slopes representing "intact" and "damaged" material.

This hypothesis is illustrated in figure 7.13 which depicts the experimental strain profile for the initial loading cycles of beam F3/2 (500/0,2). A description of the construction to determine the limit of the microcracked zone follows:-

1. The slope of the strain profile in the lowest portion of the beam (in this case between measuring positions 1 and 2) is used as representing the "fully damaged" state. The line with this slope (line A in figure 7.13) is extrapolated upwards towards the zero strain axis.

2. Provided strain at the upper measuring position (position 4) is compressive, or does not exceed approximately 100.10^{-6} of tensile strain, it is assumed that such a point lies within intact material. To obtain the slope of the strain profile for intact material, equation (7.5) is used together with the E value for intact material given in table 5.4 for the relevant

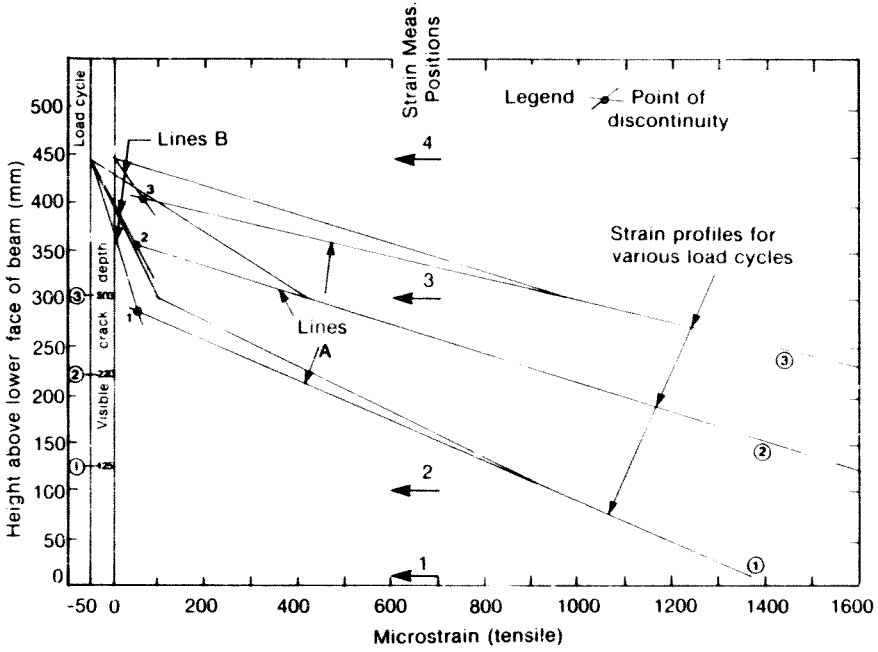

Figure 7.13 Construction to obtain microcracked zone size from experimental strain profile

beam size. The right-hand side of equation (7.5) is evaluated using the experimental h value, and then multiplied by the load maintained during the reading of the strains. The resulting value is the required theoretical slope of the strain profile. A line (line B in figure 7.13) with this slope is drawn downwards from the upper experimental strain point, to intersect line A. This intersection point is then taken as the point of discontinuity, representing the upper limit of the microcracked zone.

3. Between measuring points 3 and 4, lines of flatter slope than the theoretical lines B are shown. It is suggested that within the intact zone the theoretical line is the characteristic strain profile, which experiences a point of discontinuity with associated rapid change in slope at the upper limit of the microcracked zone. Therefore the profile given by lines B and A intersecting at the point of discontinuity is suggested as being more truly representative of the profile. The fact that only four strain measuring positions were used has probably masked the form of the strain profile, particularly in the upper portion. This is corroborated by observing tensile strain values (ε_t) of the intersection points in figure 7.13. These are approximately 55.10^{-6}, 50.10^{-6}, and 65.10^{-6}, and represent lower limits to quoted tensile strain capacities for concrete. Above these points the material will have suffered no damage, and the strain profiles would therefore be represented by lines B.

4. Also shown in figure 7.13 are positions of visible crack tips for the relevant loading cycles. The difference in height between the crack tip and the limit of the microcracked zone is the depth of this zone.

5. This method cannot be applied when the upper strain value no longer indicates an intact material, generally taken at between 100.10^{-6} to $150.10.^{-6}$ for concrete. From an experimental point of view, the method cannot be applied when the upper strain

point falls on a line of uniform slope for the balance of the profile.

The strain profiles of fifteen of the fracture beams of series F3 (three x 500mm, four x 300mm, four x 200mm, four x 100mm beams) were analysed to assess microcracked zone depths as functions of residual ligament depth h. Results are plotted in figure 7.14. For completeness, results from the ultrasonic tests are included in the figure, since they were found to conform to the same trends as the strain profile results. Chapter 8 gives details of these results. Also shown on the figure are the lines for theoretical upper and lower limits, transposed from figure 7.12. The following details apply to the results:-

1. A total of thirty-nine points (including ultrasonic results) representing the condition after visible crack growth had commenced are included. Points when the microcracked zone was still developing to its maximum size before the start of slow crack growth were excluded.

2. The majority of points come from the 300mm and 500mm beams. The strain profiles of smaller beams were more linear than those of larger beams, making assessment of microcracked zone size more difficult in these beams. In the case of 100mm beams, limited results were available because the strain profile was approximately linear and conformed to the theoretical value based on elastic modulus. The significance of this is that there was essentially no influence of the microcracked zone.

3. One experimental point falling below the lower limit is shown, but this has been excluded from the analysis on the grounds that it does not conform to the general trend. The presence of this point highlights the major difficulty with this method, which is the inaccuracy arising from a limited number of strain measuring positions.

4. The major disadvantage of the method is the sensitivity of results to the selection of a value fc On occasions, it was

found that to assess c from the mean compliance relations was better than using the visible crack depth.

5. A best-fit straight line to all the results through the origin has the following relationship:-

$$\text{Microcracked zone depth} = 0{,}463\ h \qquad (7.14)$$

6. While equation (7.14) represents all results taken together, figure 7.14 shows that results for smaller beams tend to lie closer to the lower limit than those for larger beams. Results were therefore analysed to detect whether there was a significant difference between beam sizes. It was found that 300mm and 500mm beams behaved essentially in an identical manner, with the following mean relationship:-

$$\text{Microcracked zone depth} = 0{,}470\ h \qquad (7.15)$$

The 200mm beams had the mean relationship:-

$$\text{Microcracked zone depth} = 0{,}446\ h \qquad (7.16)$$

The 100mm beams had the mean relationship:-

$$\text{Microcracked zone depth} = 0{,}401\ h \qquad (7.17)$$

At first glance the difference between the beams does not appear to be large. However, when interpreted in terms of average stress transfer in the microcracked zone, the smaller beams have lower average stresses than the larger beams since their results lie closer to the lower limit. The results for the 100mm beams in particular are an interesting corroboration of the intuitive conclusion that was made in 6.6.3. It was stated there that the influence of closing stresses in the microcracked zone would be very much less for smaller beams than larger beams, due to the greater rotations and crack surface separations occurring in smaller beams. The microcracked zone depth relationships therefore confirm this

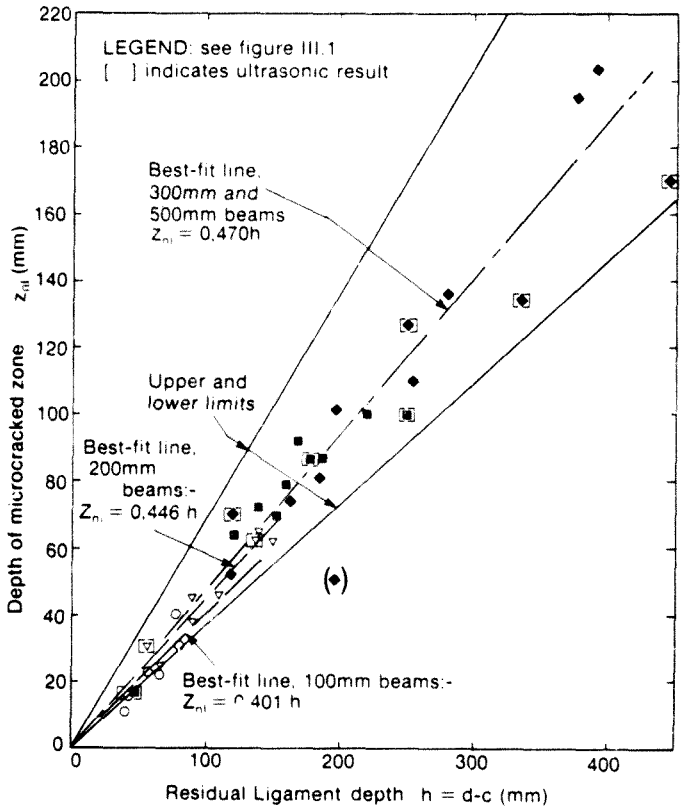

Figure 7.14 Dependence of microcracked zone size on residual ligament depth (strain profile and ultrasonic results)

conclusion when viewed in terms of the theoretical lower limit which is based on a condition of zero stress transfer. In fact, the average stresses in the microcracked zone are critically dependent on the relationship between zone depth and residual ligament depth; this aspect is more fully covered in chapter 9.

7.7 CONCLUDING REMARKS

To briefly conclude, the simple technique of strain measurement across a notched section may allow a reasonable estimate of the sizes of various fracture zones, and in particular the size of the microcracked zone. The position of the line showing the relationship between the microcracked zone size and residual ligament depth relative to upper and lower limits is characteristic of the fracture behaviour of the material. Stress transfer occurs in the microcracked zone and its magnitude will depend on beam depth.

The following chapter presents an entirely independent technique to determine microcracked zone size - the use of ultrasonic pulse velocity measurements across a section during fracture. General conclusions from chapters 7 and 8 will be drawn at the end of chapter 8.

8 FRACTURE ZONE CHARACTERISATION USING ULTRASONIC MEASUREMENTS

8.1 INTRODUCTION

The tests for series F3 involved the use of an ultrasonic technique to monitor the effects of crack growth on pulse transit time and to assess the extent of microcracking. The measurements also served as a check on microcracked zone sizes obtained from strain profiles. The ultrasonic technique for concrete has been well documented. For instance Bungey[96] referring to the use of ultrasonics in concrete states (p.35): "If properly used by an experienced operator, a considerable amount of information about the interior of a concrete member can be obtained..... Furthermore, since it is the *elastic properties of the concrete which affect pulse velocity*, it is often necessary to consider in detail the relationship between elastic modulus and strength when interpreting results". (Italics mine). Bungey's comment about the elastic modulus (E) affecting the pulse velocity is interesting, since the previous chapter has shown that the microcracked zone is characterised by a low stiffness, or a low E value. This is the basis on which the method has been used to detect microcracking in the present work. Blight[97] also used the technique to study cracking in concrete caused by alkali-aggregate reaction. He found the technique excellent for detecting damage such as microcracking or the presence of voids, although the ability of the method to determine the strength of the concrete was questionable. For the present tests strength was not the issue, and the method was used primarily to

see whether it was sensitive to development of fracture zones in a beam.

Details of the equipment and method of measuring transit times have been given previously in 4.4 and 4.5. The ultrasonic test data comprised longitudinal pulse transit times t (in microseconds) at the various measuring positions for the load cycles during a test. Figure 4.4 gives details of the measuring positions. Preliminary tests showed that the technique was insensitive to pulse measurements across the beam width, and that greater consistency could be maintained by measuring at the end of any load cycle.

The ultrasonic test results were used in two ways:- firstly to assess the development of microcracked zones ahead of the main (visible) crack tip, and secondly to assess crack growth by means of increase in pulse transit times. These two aspects will be dealt with in order.

8.2 DEVELOPMENT OF MICROCRACKED FRACTURE ZONES

The ultrasonic measurements were analysed and are presented in figures 8.1 to 8.4. These figures were intended to explore the ability of the method to detect development of microcracked zones. The ordinate axis represents the depth of the visible crack (including the initial notch depth), while the abscissa axis represents the change in pulse transit time Δt during a test (i.e. the initial transit time differenced from the succeeding times measured during a test). In this way, influence of crack growth on transit time could be studied, from which changes in concrete microstructure could be inferred.

The figures show the same general trend of steadily increasing rate of change of transit time with increasing crack growth. The curves are for the different measurement positions, shown on the diagram. The curve for position 2 has been omitted for clarity, and because

it is very similar to that for position 1. Only experimental points for certain measuring positions have been shown, other points being omitted again for clarity. For any given position a scatter of results has occurred. This is to be expected when the ultrasonic technique is used to assess fairly small changes in transit time due to changes in the internal state of the concrete. For instance, changes in transit time varied from 2,5 per cent to 8,3 per cent of initial readings, with the greatest changes occurring at the lower measuring position 1. Clear trends were evident which allowed curves to be drawn, but the limitations in making quantitative deductions should not be forgotten.

The following points may be noted:-

1. There is no distinction between experimental points with respect to initial notch depth, since it was clear during plotting that curves were independent of notch depth. The initial points for a more deeply notched beam began nigher up, but fell along the same curve as the points for shallower notch depths. Therefore a visible crack at any particular height was having the same effect on concrete microcracking irrespective of the proportion of the crack depth made up by the notch. It could therefore be expected that the extent of microcracking ahead of the visible crack would be dependent only on crack depth for a particular size of beam.

2. Referring to measurement positions initially above the notch, the figures show that the change in transit time is sensitive to the approach of a microcracked zone. Considering the curve for position 6 in figure 8.1, there is little change in transit time initially as the main crack propagates upwards from the notch. This is followed by an increasing rate of change of transit time with crack growth indicating that the approaching crack is exercising an effect due to the zone of damage or microcracking that has developed ahead of the main crack. Regarding position 5, the crack exercises a significant effect at this fairly high position at an early stage during the load cycling. These curves deviate from the vertical axis at posi-

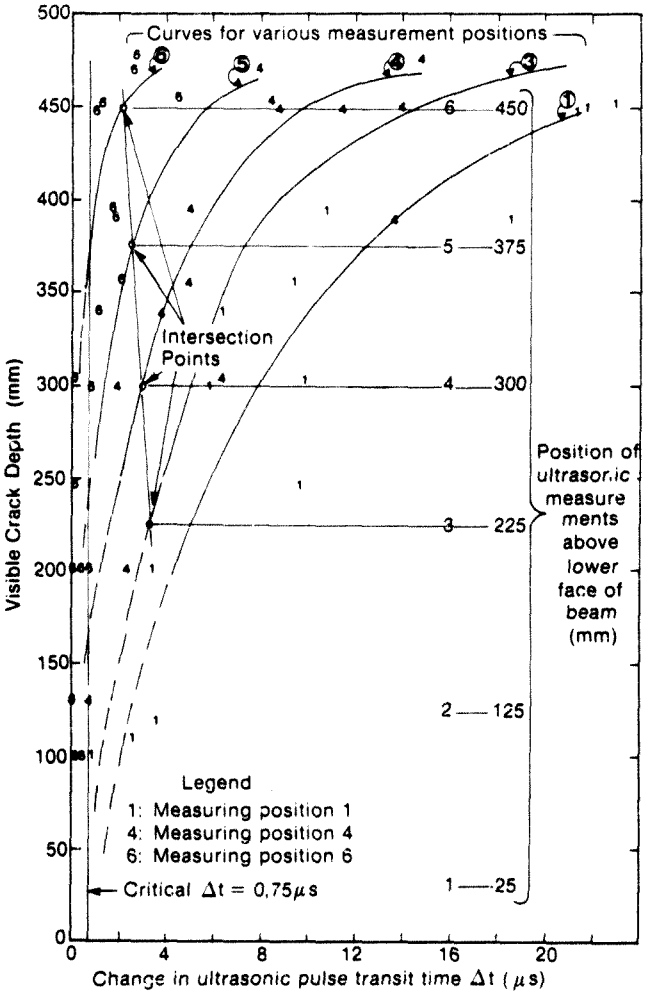

Figure 8.1 Effect of crack growth on ultrasonic pulse transit time, 500mm beams

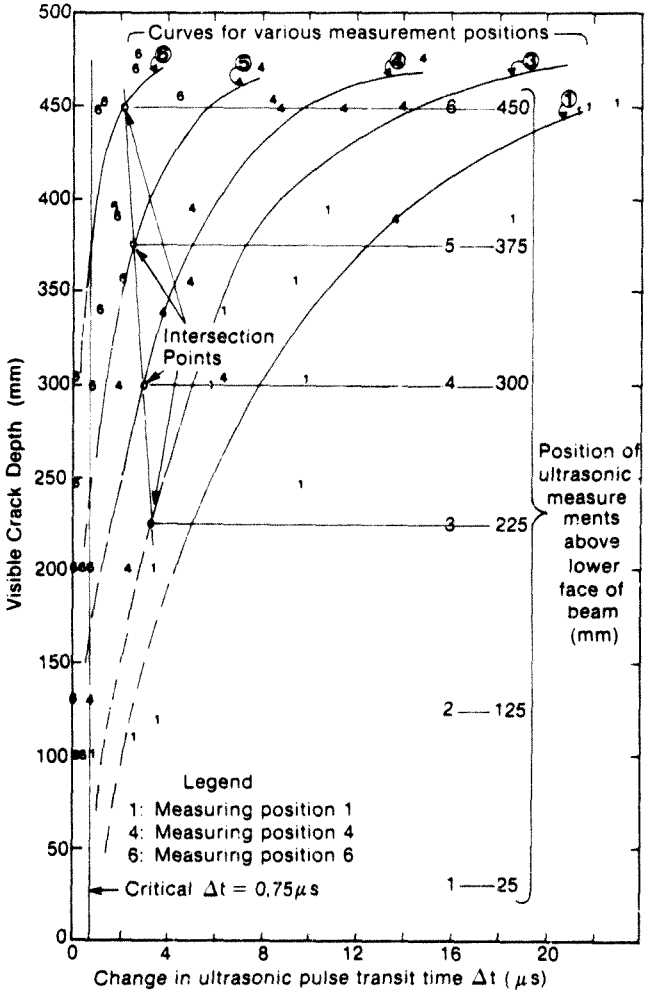

Figure 8.1 Effect of crack growth on ultrasonic pulse transit time, 500mm beams

tions well below the respective measuring positions which indicates the approach of a microcracked zone.

3. Referring to measurement positions initially below the notch, for example position 1 in figure 8.2, there is a rapid change in transit time during initial loading with very little or no change in visible crack depth. This is shown by the horizontal lines at notch positions of 75mm and 120mm, and indicates again the development of a zone of microcracking. Once the crack starts growing, the change in transit time (Δt) will indicate change in crack depth since Δt will be much more sensitive to a change in stress-free crack depth across which a pulse cannot transmit than to a change in size of a microcracked zone across which pulse transmission can still occur. Hence, it might be expected that a curve such as that for position 1 will be useful for estimating the stress-free crack depth. This point receives further attention in 8.3 below, where the questions of influence of crack width on transit time and ability of the microcracked material to transmit an ultrasonic pulse are also considered. Suffice to say at this point that a damaged material can still transmit pulses even though they are somewhat attenuated.

4. The increasing rate of change of pulse time t with crack depth c shown in the curves indicates that a given increment in c initially has a small effect on t, particularly for measuring positions higher in the beam. The visible crack is well below the measuring position, and the pulse is sensing a small change in the degree of microcracking. Near the end of the curve, however, a given increment in c has a large effect on t. The crack has intersected the measuring position and pulse time is critically affected by the relatively large increase in pulse path length, caused by increase in crack depth. As the crack approaches the upper face of the beam, transit time is also affected by the rapid reduction of the area of "intact" material through which the pulse can travel.

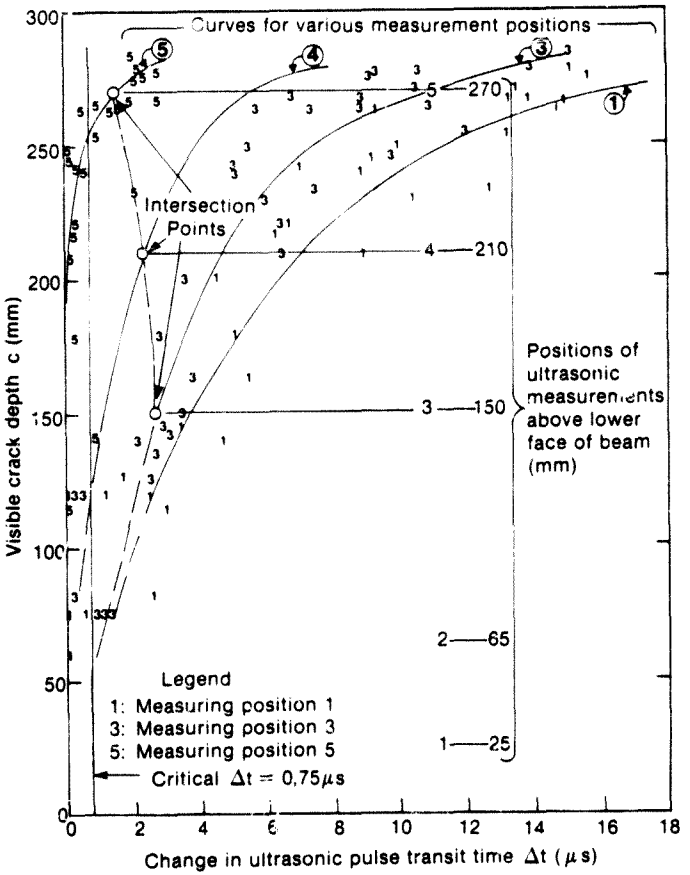

Figure 8.2 Effect of crack growth on ultrasonic pulse transit time, 300mm beams

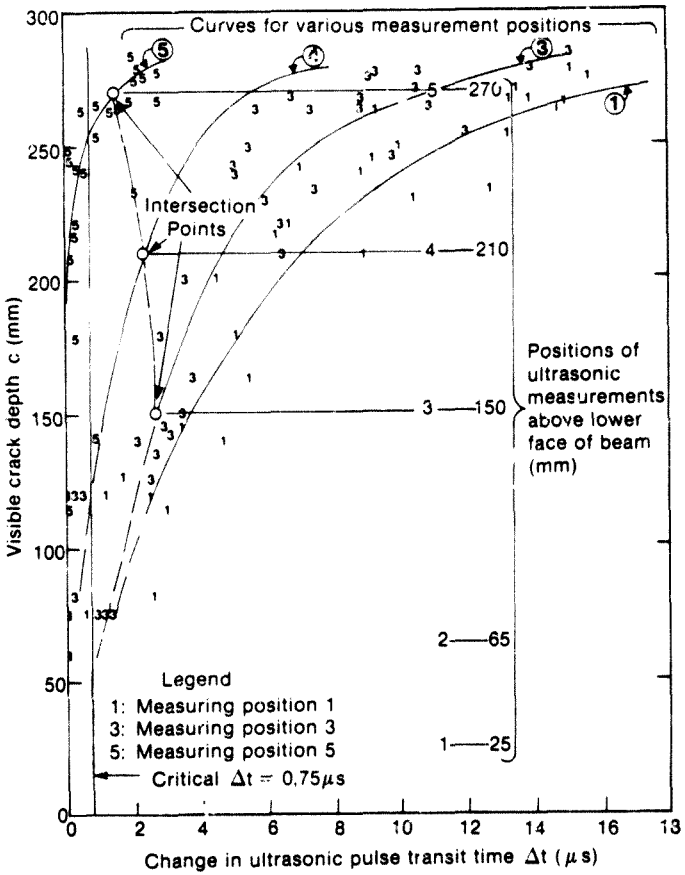

Figure 8.2 Effect of crack growth on ultrasonic pulse transit time, 300mm beams

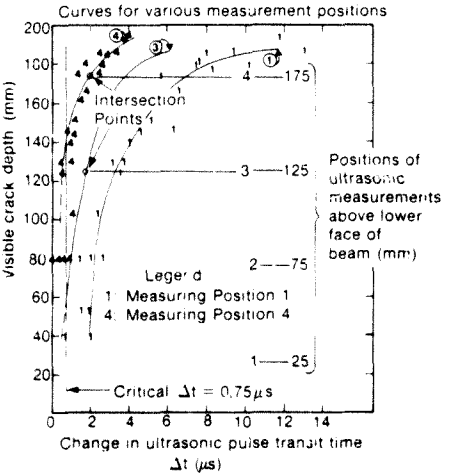

Figure 8.3 Effect of crack growth on ultrasonic pulse transit time, 200mm beams

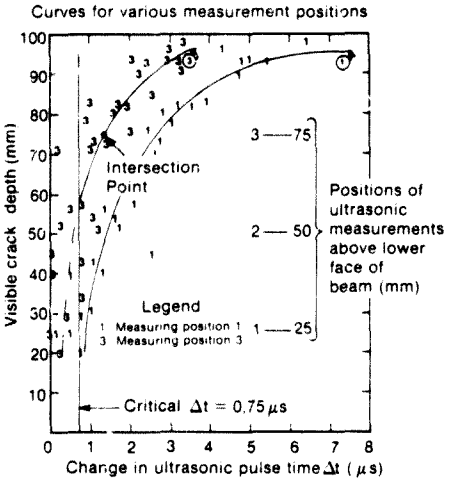

Figure 8.4 Effect of crack growth on ultrasonic pulse transit time, 100mm beams

5. Points called "intersection points" are also shown on the curves, i.e. those points when the visible crack crosses over or intersects the measuring position. The locus of intersection points shows that the total Δt generally increases as the measuring position moves downwards from the highest position in the beam. Assuming the advance of the stress-free crack tip itself will reduce the pulse time at a measuring position by an equal amount irrespective of that position, then the total change in transit time at any intersection point must be a measure of the intensity of microcracking. Interpreting this for the intersection points in figure 8.2, the sketch in figure 8.5 gives a schematic representation of microcracking at the various measuring positions. The intensity of microcracking and zone size are greater for position 3 than for positions 4 or 5.

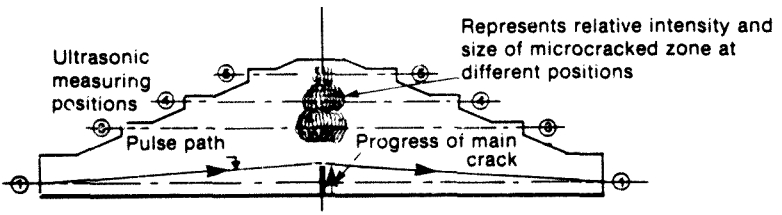

Figure 8.5 Schematic representation of microcracking at ultrasonic measuring positions, 300mm beam

Examination of the locus of intersection points in figures 8.1 and 8.2 also indicates that the points for curves 1 and 2 (although curve 2 has been omitted) would lie closer to the ordinate axis than the point for curve 3. This means that for these positions relative to the notch depths, the microcracked zone is not able to reach its maximum potential size before the main crack starts growing. If the notch depths had been shallower, or even zero, the curves for these positions would have shifted outwards from the ordinate axis. Since the stress-intensity factor (and hence the intensity and size of the highly stressed zone) is a function not only of applied load but also of crack depth, it is feasible that the microcracked zone

5. Points called "intersection points" are also shown on the curves, i.e. those points when the visible crack crosses over or intersects the measuring position. The locus of intersection points shows that the total Δt generally increases as the measuring position moves downwards from the highest position in the beam. Assuming the advance of the stress-free crack tip itself will reduce the pulse time at a measuring position by an equal amount irrespective of that position, then the total change in transit time at any intersection point must be a measure of the intensity of microcracking. Interpreting this for the intersection points in figure 8.2, the sketch in figure 8.5 gives a schematic representation of microcracking at the various measuring positions. The intensity of microcracking and zone size are greater for position 3 than for positions 4 or 5.

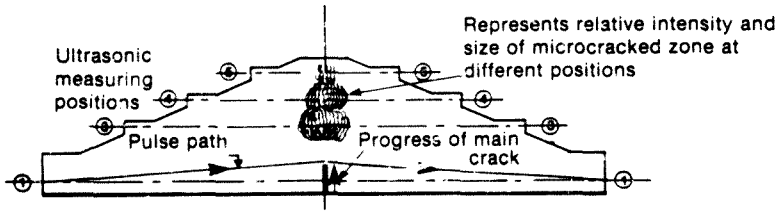

Figure 8.5 Schematic representation of microcracking at ultrasonic measuring positions. 300mm beam

Examination of the locus of intersection points in figures 8.1 and 8.2 also indicates that the points for curves 1 and 2 (although curve 2 has been omitted) would lie closer to the ordinate axis than the point for curve 3. This means that for these positions relative to the notch depths, the microcracked zone is not able to reach its maximum potential size before the main crack starts growing. If the notch depths had been shallower, or even zero, the curves for these positions would have shifted outwards from the ordinate axis. Since the stress-intensity factor (and hence the intensity and size of the highly stressed zone) is a function not only of applied load but also of crack depth, it is feasible that the microcracked zone

grows to a maximum in size and intensity before main crack growth occurs, and then reduces again as the residual ligament depth reduces. A wider range of shallow notch depths should be studied to further corroborate this.

6. A measure of the vertical depth of a microcracked zone can be obtained from the ordinate scale distance between any particular measuring position and the point below at which the respective curve deviates significantly from the ordinate axis. The problem here is to determine the change in transit time that actually represents significant onset of microcracking. Results for highest positions in the beams showed that Δt fluctuated about the zero position during initial crack growth, and these fluctuations were random and not significant. At some point during crack growth, Δt became significant as the zone of microcracking began to develop at the measuring position. The random Δt fluctuations were about 0,5 μs, and the assumption is therefore that a value above 0,5 μs can be taken as significant.

The problem of determining significant Δt was investigated by testing three elastic modulus prisms from series F3 in uniaxial compression. Ultrasonic pulse times were noted across the two horizontal axes at mid-height during the tests. The prisms were loaded at a steady rate of about 2,5MPa/min. Results were expressed in terms of stress as percentage of failure stress and mean change in ultrasonic pulse transit time Δt; see figure 8.6. Note that the type of failure induced at mid-height of the prism was vertical cracking, and therefore was similar to the type of microcracking occurring in fracture beams.

It is generally accepted (see for instance Illston et al[88]) that significant change in ultrasonic pulse time occurs at about 70 to 80 per cent of uniaxial compressive failure stress for normal strength concrete. From figure 8.6 it can be seen that the critical Δt is between about 0,5μs and 1μs (although one prism gives a value at 80 per cent in excess of 2 μs). Taking the two prisms with similar results, a significant Δt of 0,75μs is selected. This also

coincides with the point where rapid change of slope begins to occur.

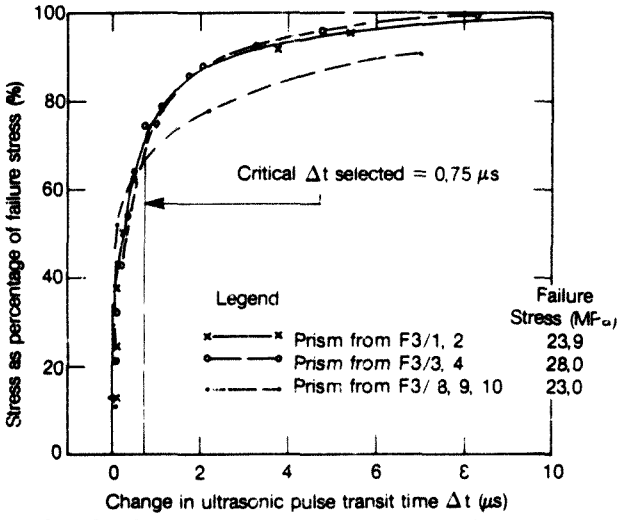

Figure 8.6 Results of prism compression tests to determine significant change in ultrasonic pulse transit time

Applying this critical value to the results shown in figures 8.1 to 8.4, microcracked zone depths can be deduced. The analysis is presented in table 8.1. Figure 8.7 presents the results in terms of the residual ligament depth.

Before discussing the results, it should be stressed that the numbers given for microcracked zone size are a rough guide, due to the spread of results which made it difficult to define the curves in figures 8.1 to 8.4 accurately, and also due to the critical dependence of zone size on the Δt value selected as being significant. (Refer to the very steep slopes of the curves in the region Δt = 0,5μs to 1μs). Figure 8.7 shows a marked and roughly linear dependence of zone depth on residual ligament depth. The most significant aspect of figure 8.7, however, is that it confirms the results for microcracked zone size obtained from strain profiles.

coincides with the point where rapid change of slope begins to occur.

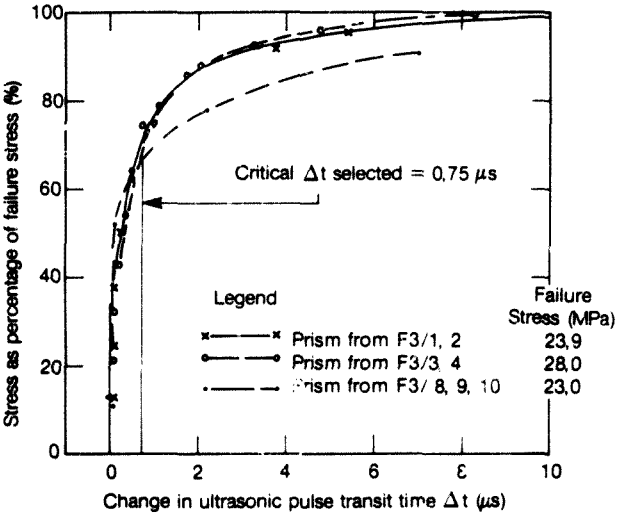

Figure 8.6 Results of prism compression tests to determine significant change in ultrasonic pulse transit time

Applying this critical value to the results shown in figures 8.1 to 8.4, microcracked zone depths can be deduced. The analysis is presented in table 8.1. Figure 8.7 presents the results in terms of the residual ligament depth.

Before discussing the results, it should be stressed that the numbers given for microcracked zone size are a rough guide, due to the spread of results which made it difficult to define the curves in figures 8.1 to 8.4 accurately, and also due to the critical dependence of zone size on the Δt value selected as being significant. (Refer to the very steep slopes of the curves in the region Δt = 0,5μs to 1μs). Figure 8.7 shows a marked and roughly linear dependence of zone depth on residual ligament depth. The most significant aspect of figure 8.7, however, is that it confirms the results for microcracked zone size obtained from strain profiles.

Table 8.1 Assessment of depth of microcracked zones as a function of residual ligament depth, from ultrasonic measurements

Beam depth d (mm)	Measuring position	Visible crack depth c (mm)	Depth of microcracked zone (mm)	h=(d-c) (mm)
500	3	55	170	445
	4	165	135	335
	5	248	127	252
	6	380	70	120
300	3	50	100	250
	4	123	87	177
	5	253	17	47
200	3	62	63	138
	4	144	31	56
100	3	58	17	42

(Note that results shown in figure 8.7 have been previously shown in figure 7.14, in order to compare ultrasonic results with strain profile results). The upper and lower zone limits determined in 7.5.3, as well as the mean line for the strain profile results, are shown on the figure. The ultrasonic results fall within the zone limits, and the mean line lies close to the strain profile line, the difference between the two being about 7 per cent. The mean line for the ultrasonic results has the equation:-

$$\text{Microcracked zone depth} = 0{,}439h \qquad (8.1)$$

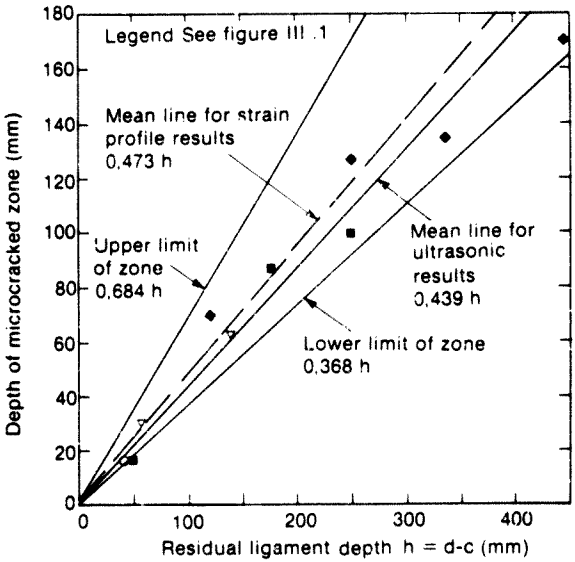

Figure 8.7 Dependence of microcracked zone depth on residual ligament depth, from ultrasonic measurements

As mentioned previously, the ultrasonic results are critically dependent on the choice of significant change in pulse transit time. Had a value less than 0,75μs been adopted, the microcracked zone size would have been larger. Within the limits of accuracy of the ultrasonic method, results have been obtained that conform remark-

ably well to those obtained using an entirely independent method, and have shown the value of this technique in fracture studies.

The dependence of microcracked zone size on uncracked ligament depth h is further illustrated by comparing the total change in transit time Δt for similar h values for the 300mm and 500mm beams. Thus measuring position 5 (500mm beams) has h = 125mm, while position 3 (300mm beams) has h = 150mm. At these positions, the Δt value at the intersection points are 2,6μs and 2,7μs respectively. Similarly, position 6 (500mm beams) has h = 50mm and Δt (intersection point) = 2,1 μs, while the average between positions 4 and 5 (300mm beams) has h = 50mm and Δt (average between intersection points) = (1,5+2,4)/2 = 2μs. The correspondence between these values indicates again the similarity in microcracked zone size for any given residual ligament depth.

8.3 ASSESSMENT OF CRACK DEPTH FROM ULTRASONIC PULSE MEASUREMENTS

It has been mentioned previously that for an ultrasonic measuring position below a crack tip the change in pulse transit time is mainly sensitive to stress-free crack depth (rather than microcracked zone size). The curves for position 1 in figures 8.1 to 8.4 show that, after a small initial Δt due to microcracked zone development, the subsequent Δt values are critically dependent on visible crack growth c which causes an increase in pulse path length. This deduction allows an estimate of the stress-free crack depth to be made from the pulse transit times measured at positions below the crack tip.

Before the method is discussed, it is necessary to present and discuss the results of a subsidiary test that was done to confirm that pulse transit time was being influenced by path length (and hence crack depth) and not crack width. Details of this test are:-

1. One half of previously fractured beam F3/16 (200/0,4) was prepared by facing the fractured end to produce a smooth flat surface for the ultrasonic probe, and cutting an 81mm notch in the centre of the beam. The beam was 412mm long after preparation.

2. One set of "demec" strain targets was fixed at mid-height of the beam (i.e. 100mm above the lower face) and straddling the beam mid-span in order to measure crack width.

3. Ultrasonic readings were taken at two positions i.e. 25mm and 100mm above the lower face of the beam. The readings at the 100mm position were used to check the effect of crack width, while those at the 25mm position were used to check the effect of crack depth.

4. The beam was placed on a 20mm x 110mm x 450mm steel plate using an interface of 20mm thick timber chipboard, and loaded on a 400mm span using rollers set at 100mm loading span. A separate piece of chipboard was used under each half of the beam, and this material was used to create an "ultrasonic barrier" between the concrete beam and the steel plate. The chipboard had a density of 676kg/m^3 which meant that the pulse would preferentially transmit through the denser concrete. The steel plate was used to control the fracture of the concrete beam.

5. Once an initial crack had grown from the notch the load was removed and the crack width increased by wedging open the notch faces. Thus the crack was extended in a stable fashion and the crack width continually increased. When the crack was within a few millimetres of the upper beam face, a clamp acting through small timber bearers was used to prevent complete separation of the beam halves.

6. Eventually, the clamp was removed in order to allow complete separation of beam halves, which were gradually moved apart while readings of "crack width" (i.e. effectively crack face

1. One half of previously fractured beam F3/16 (200/0,4) was prepared by facing the fractured end to produce a smooth flat surface for the ultrasonic probe, and cutting an 81mm notch in the centre of the beam. The beam was 412mm long after preparation.

2. One set of "demec" strain targets was fixed at mid-height of the beam (i.e. 100mm above the lower face) and straddling the beam mid-span in order to measure crack width.

3. Ultrasonic readings were taken at two positions i.e. 25mm and 100mm above the lower face of the beam. The readings at the 100mm position were used to check the effect of crack width, while those at the 25mm position were used to check the effect of crack depth.

4. The beam was placed on a 20mm x 110mm x 450mm steel plate using an interface of 20mm thick timber chipboard, and loaded on a 400mm span using rollers set at 100mm loading span. A separate piece of chipboard was used under each half of the beam, and this material was used to create an "ultrasonic barrier" between the concrete beam and the steel plate. The chipboard had a density of 676kg/m^3 which meant that the pulse would preferentially transmit through the denser concrete. The steel plate was used to control the fracture of the concrete beam.

5. Once an initial crack had grown from the notch the load was removed and the crack width increased by wedging open the notch faces. Thus the crack was extended in a stable fashion and the crack width continually increased. When the crack was within a few millimetres of the upper beam face, a clamp acting through small timber bearers was used to prevent complete separation of the beam halves.

6. Eventually, the clamp was removed in order to allow complete separation of beam halves, which were gradually moved apart while readings of "crack width" (i.e. effectively crack face

separation) and transit time were taken. The beam halves were then pushed together and final readings taken.

Results from the subsidiary test and series F3 tests are shown in figures 8.8 to 8.10.

FIGURE 8.8

This shows the effect of crack width (at mid-height of the beam) on ultrasonic pulse measurements, as recorded in the subsidiary test. Three distinct portions of the curve are identifiable:-

1. An initial portion up to a crack width of about 850μm and a crack depth of 190mm, in which the change in pulse time is small (less than about 6μs). This indicates that crack width is essentially having no effect on ultrasonic measurements. This portion of the curve would apply to the tests conducted in series F3.

2. An intermediate portion where a significant "step" in pulse time occurs, followed by a roughly vertical line (i.e. between crack widths of 850μm to 6000μm, and crack depths of 190mm to 197mm). The important feature here is the close approach of the crack to the upper beam surface, leaving very little residual ligament depth. Due to the large rotation of the beam, the remaining ligament material would be extensively damaged and this is considered to be the main cause for the "step" in the curve at the beginning of this portion. What is also significant, however is the ability of the extensively damaged material to still transmit an ultrasonic pulse.

3. A final portion where complete separation of crack faces has occurred, and change in pulse time becomes very large. This portion represents the pulse being transmitted from the concrete through the chipboard and steel plate successively. The fact that the pulse time increases so dramatically between the conditions of beam contact and beam separation shows that the

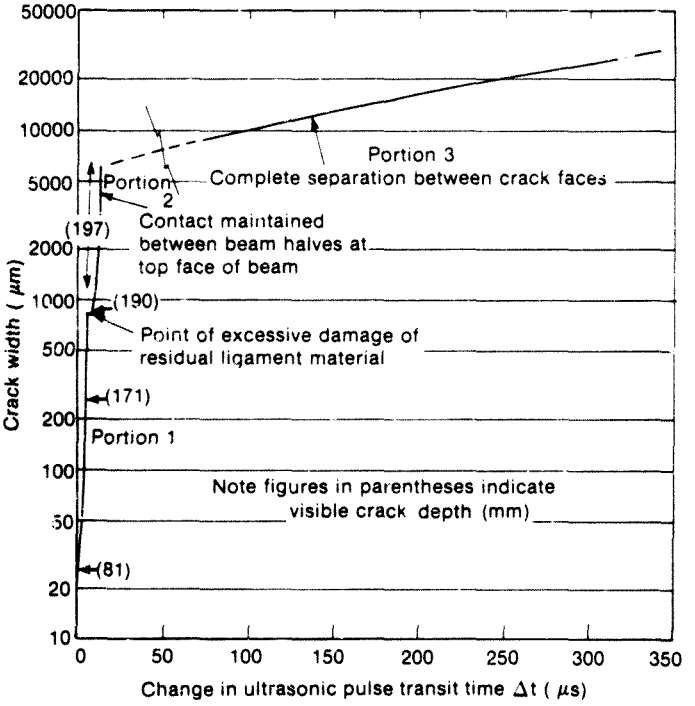

Figure 8.8 Effect of crack width on ultrasonic pulse transit time

first two portions of the curve represent the pulse transmitting preferentially through the concrete rather than the timber or steel.

The final change in pulse transit time at the end of the test when the two beam halves were pushed together was 9,4μs, which corresponds roughly with the final condition of portion 2. This again showed the ability of the pulse to pass through highly damaged material at residual points of contact.

The main conclusion to be drawn from figure 8.8 is that change in pulse transit time is not sensitive to crack width, but is affected by the state (i.e. whether intact or damaged) of the residual ligaments through which the pulse has to pass. The question of dependence of transit time on path length is now discussed with reference to figures 8.9 and 8.10.

FIGURE 8.9

This figure shows the relationship between path length and pulse transit time for series F3, and was produced as follows:-

1. The path lengths were computed from the formula:-

$$r = 2\left[(c-y)^2 + (L/2)^2\right]^{\frac{1}{2}} \qquad (8.2)$$

where

r is the ultrasonic path length (mm)
c is the visible crack depth (mm)
y is the height (in mm) of the ultrasonic measuring position above the lower face of the beam
L is the direct horizontal distance through the beam between the ultrasonic probes.

The formula assumes a direct triangular path for the ultrasonic pulse around the visible crack tip. (See the path length shown in figure 8.5).

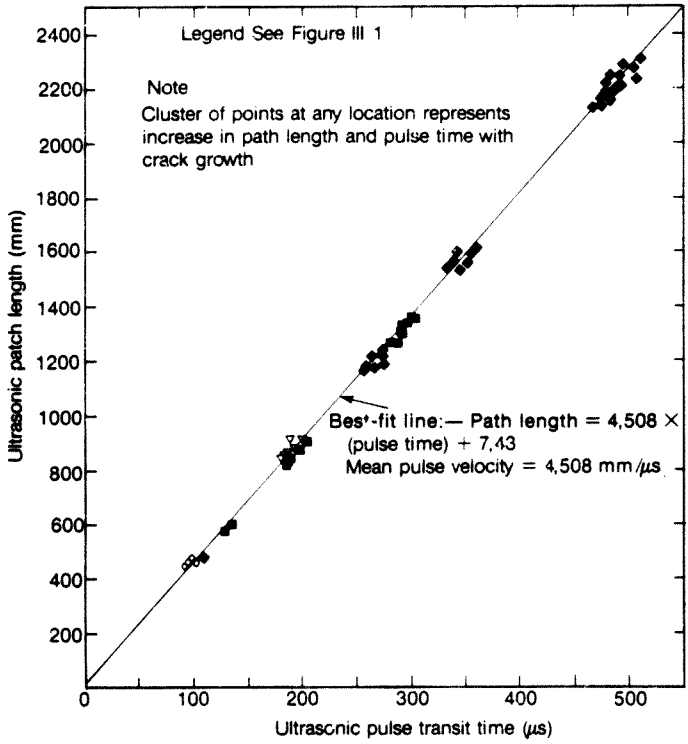

Figure 8.9 Dependence of ultrasonic pulse transit time on path length

2. The pulse transit times were those directly recorded in the tests.

The full range of representative beams of series F3 were analysed to produce figure 8.9 using the various measuring positions. A cluster of points therefore represents a particular measuring position for a particular beam size, and shows increase in path length and pulse time occasioned by crack extension. Results for all beam sizes fall on a straight line, and the degree of fit is remarkably good. We can conclude that concrete quality for all beams was consistent, but more importantly that pulse time was directly related to path length. Crack growth gave rise to increases in path length and pulse time which plotted directly along the straight line relationship. The mean pulse velocity from this relationship was 4,508mm/μs.

FIGURE 8.10

The figure gives details of results for 500mm beams (and the subsidiary 200mm test beam referred to previously). It is therefore a magnification of the topmost cluster of points in figure 8.9, and reinforces the conclusion that the change in ultrasonic pulse time results from a change in path length which itself is caused by crack extension. The best-fit relationship for the 500mm beams lies very close to the overall relationship for all the beams. Results for the subsidiary test follow the same trend as the previous tests.

Results of the main series of ultrasonic tests as well as the subsidiary test show conclusively that pulse transit time is dependent on path length rather than crack width. The path length in turn is affected by crack depth, and computing path length as the direct triangular path around the visible crack tip gives good results. This fact is used below to compare visible crack depths with crack depths predicted from ultrasonic measurements.

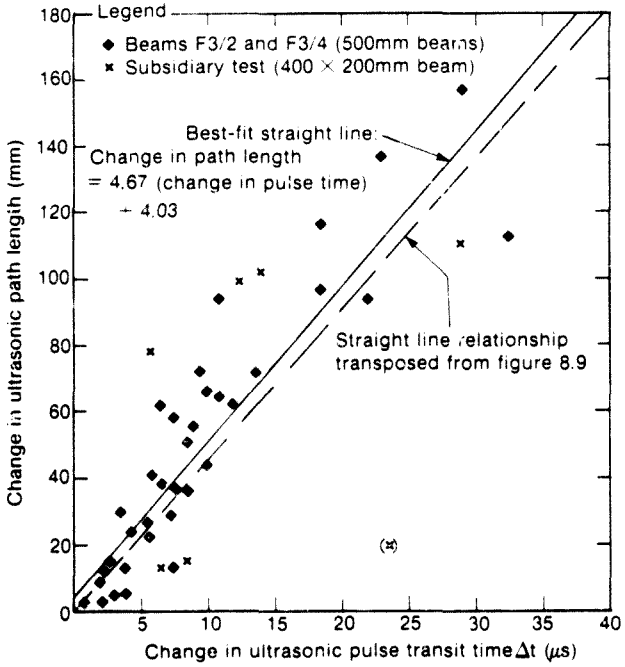

Figure 8.10 Relationship between change in ultrasonic path length and pulse time for 500mm beams

Results for 500mm and 300mm beams of series F3 were analysed to assess crack depths from ultrasonic measurements. Figure 8.9 shows that a direct relationship exists between path length and pulse time, but it is instructive to re-work the data in the form of crack depths inferred from changes in pulse transit times. The basis of the method has been given above, but is summarised below for clarity. Ultrasonic measurements at position 1 are being referred to.

1. Since there is a geometrical relationship between crack depth and path length, and a velocity relationship between path

length and transit time, the transit time can be taken as a measure of crack depth.

2. An estimate of ultrasonic pulse velocity for any beam is obtained from the initial transit time reading (μs) and the known path length (mm) calculated using the known initial notch depth. (Using this pulse velocity gave better results than using the overall mean velocity given in figure 8.9).

3. Increases in transit time during the test are interpreted in terms of increased path lengths using the new transit times and the pulse velocity calculated from the initial reading. The increased path lengths can than be converted directly to crack depths using the inverse form of equation (8.2).

An example of a calculation is given below:-

BEAM F3/5(300/0,2) (L = 1275mm)

Initial transit time reading t = 283,5μs.
Initial notch depth = 60mm.
Since the probe position is 25mm above the lower face of the beam, the effective crack depth for the calculation is 60-25 = 35mm. For this crack depth, the initial pulse path length (r_i) from equation (8.2) is:-

$$r_i = 2\left[(60-25)^2+637,5^2\right]^{\frac{1}{2}} = 1276,9\text{mm}$$

Therefore, the initial pulse velocity v_i is

$$v_i = \frac{r_i}{t} = 4,504\text{mm}/\mu\text{s}$$

The test results and interpretation are given in table 8.2.

Table 8.2 Prediction of crack depths for beam F3/5(300/0,2)

Load cycle	Transit time t (μs)	Path length $r=v_i t$ (mm)	Predicted crack depth c_u (mm)	Measured crack depth c (mm)
0*	283,5	1276,9	60	60
1	288,2	1298,1	147	141
3	296,2	1334,1	221	233
6	302,1	1360,7	263	277

* initial reading

(Note Predicted crack depth = $0,5\sqrt{r^2-L^2}$ + 25 (mm) for measuring position 1, where L=1275mm)

Similar calculations were performed for all 500mm and 300mm beams of series F3. Results are plotted in figure 8.11. Comments are as follows:-

1. A total of sixty-three experimental points are plotted. The spread of results was unaffected by initial notch depth ratio.

2. There is a general tendency for the ultrasonic method to overpredict during early stages of crack growth and to underpredict at later stages. The best-fit straight line (linear regression) has the equation:-

$$c_u(\text{mm}) = 0,83c + 23,3 \qquad (8.3)$$

where c_u is the crack depth obtained from ultrasonic measurements, and c is the visible crack depth. The point of equality is at $c_u = c = 137$mm. In practical terms, this means that for 300mm beams the average overprediction for $60 < c < 137$mm will

Table 8.2 Prediction of crack depths for beam F3/5(300/0,2)

Load cycle	Transit time t (μs)	Path length $r=v_i t$ (mm)	Predicted crack depth c_u (mm)	Measured crack depth c (mm)
0*	283,5	1276,9	60	60
	288,2	1298,1	147	141
3	296,2	1334,1	221	233
6	302,1	1360,7	263	277

* initial reading

(Note Predicted crack depth = $0,5\sqrt{r^2-L^2}$ + 25 (mm) for measuring position 1, where L=1275mm)

Similar calculations were performed for all 500mm and 300mm beams of series F3. Results are plotted in figure 8.11. Comments are as follows:-

1. A total of sixty-three experimental points are plotted. The spread of results was unaffected by initial notch depth ratio.

2. There is a general tendency for the ultrasonic method to overpredict during early stages of crack growth and to underpredict at later stages. The best-fit straight line (linear regression) has the equation:-

$$c_u(mm) = 0,83c + 23,3 \qquad (8.3)$$

where c_u is the crack depth obtained from ultrasonic measurements, and c is the visible crack depth. The point of equality is at $c_u = c = 137mm$. In practical terms, this means that for 300mm beams the average overprediction for 60 < c < 137mm will

be approximately 11 per cent, while the average underprediction for 137 < c < 275mm will be approximately 4,3 per cent. The corresponding numbers for the 500mm beams will be:-

100 < c < 137mm	:-	approximately 3 per cent overprediction.
137 < c < 450mm	:-	approximately 6 per cent underprediction.

Hence, the ability of this simple prediction method based on ultrasonic readings is remarkably good.

3. The reason for overprediction of crack depth at early stages of crack growth can be found in the initial development of a microcracked zone before advance of the main crack tip; the effect of this zone is to cause an increase in the ultrasonic pulse transit time. Once the microcracked zone has developed, the main crack advances and the readings reflect this crack advance. It would be possible to refine the method to include for the effect of the microcracked zone, but in view of the reasonable fit of results this may not be worthwhile practically.

4. The reason for underprediction of crack depth at later stages of crack growth can probably be found in the difference between the depth of the visible crack observed experimentally, and the depth of a true stress-free crack. It is feasible that for some distance behind the visible crack tip stress transfer still occurred, and the ultrasonic pulse could transmit across the crack behind the visible crack tip. In this case, the predicted crack depth will be less than the observed depth.

5. The trend of figure 8.11 is actually a magnified reflection of the points shown in figure 8.9. Thus, the topmost cluster of points in figure 8.9 generally lie slightly above the mean line, meaning that pulse times were slightly lower than the mean line would predict. This cluster of points corresponds with the larger values of crack depth in figure 8.11. Therefore using

the pulse times will cause slight underprediction of crack depth. Conversely, the cluster of points corresponding to the lower values of crack depth in figure 8.11 (for the 300mm beams) is that lying at path length = 1275mm and slightly above. These points generally lie slightly below the mean line; applying similar reasoning this means that using pulse times will cause slight overprediction of crack depth.

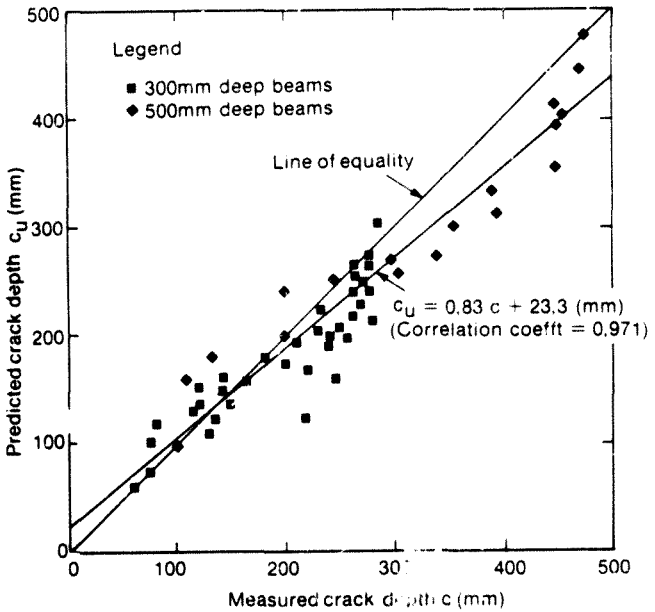

Figure 8.11 Comparison of measured and predicted crack depths using an ultrasonic technique

6. The limitations of the method described above should be clearly appreciated. They are briefly:-

   a. A small error in pulse transit time measurement will lead to a large error in predicted crack depth. For instance, a 1 per cent error in transit time will lead typically to

a 12 per cent error in crack depth, although the effect of the error is magnified during the very early stages of crack growth when an error of 60 per cent in crack depth might typically result from a 1 per cent error in transit time. However, it is generally possible to read ultrasonic transit time to within 0,1 per cent which implies that the likely errors in crack depth will range from about 1 per cent to about 6 per cent.

b. Since the predicted crack depths have been compared with observed crack depths, the accuracy of the prediction will depend on the accuracy of crack tip observation. As noted previously in 4.5.2, this depends very much on the scale effect of specimen size and on optical equipment. It was felt that the reasonable correlation between observed and predicted crack depths lent considerable weight to the technique of visual observation of the cracks.

5.4 CONCLUSIONS FROM ULTRASONIC TESTS

The main conclusions are:

1. The ultrasonic technique is useful for assessing development of fracture zones and for estimating the size of such micro-cracked zones in fracture beams. Results show good correlation with those obtained from the analysis of strain profiles.

2. The technique is able to detect crack growth by the effect this growth has on pulse path length. The method can therefore be used to predict crack depth, account being taken of the tendency to overpredict at smaller depths and underpredict at greater depths.

3. The main problems with the ultrasonic method have to do with the accuracy of the method (i.e. the scatter of results that

occurs), and the selection of a suitable value for significant change in pulse transit time.

9.5 GENERAL CONCLUSIONS FOR MEASUREMENT OF FRACTURE ZONES

Referring to discussion in chapters 7 and 8, the following general conclusions may be drawn:-

1. Distinct stress zones may be identified in concrete fracture beams. For fracture studies, knowledge of the stress states of these zones, and in particular the microcracked zone, is essential. Chapters 7 and 8 present the results of two experimental techniques - strain measurement and ultrasonic pulse measurement - that were used successfully to measure fracture zones.

2. Strain and displacement profiles in notched sections show marked non-linearity, leading to distortion of plane sections. This distortion is intensified as beam depth increases and arises from the development of a microcracked zone ahead of the stress-free crack tip. Material behind the upper limit of the microcracked zone has suffered damage which imparts to it a lower effective stiffness than intact material ahead of the zone. It was found that the effective stiffness (E value) of deeper beams was reduced more than that of shallower beams, indicating the greater notch-sensitivity of these beams.

3. Values of crack opening displacement (COD) at visible crack tips were found to increase as beam depth increased, being on average about 37μm for the 100mm beams and 64μm for the 500mm beams.

4. The effect of the microcracked zone on neutral axis position is to cause this position to shift up very rapidly during early

stages of crack growth. A constant relation between tension and compression zone sizes is maintained during subsequent crack growth. The neutral axis was found to fall at a position above the crack tip roughly two-thirds of the distance between the crack tip and the upper face of the beam.

5. The relation between compression and tension zone sizes could be considered characteristic of the fracture behaviour of the particular material being tested. The present concrete was found to be inelastic and quasi-ductile in the sense that for the tension zone there is considerable non-linearity in strain and stress profiles and the presence of a microcracked zone prevents truly brittle behaviour from occurring.

6. Experimental relationships between compression and tension zone sizes allow "theoretical" upper and lower limits for the microcracked zone as functions of residual ligament depth to be predicted. These limits are:-

   Upper limit = 0,684 (d-c)
   Lower limit = 0,368 (d-c)

   These limits provide a framework within which to evaluate measurements and calculations of microcracked zone size.

7. Distortion of the strain profile can be used to assess the extremity of the microcracked zone. This was found to be on average about 46 per cent of residual ligament depth, taking strain profile and ultrasonic results together. However, it appeared that the size of the microcracked zone depended on beam size, 100mm beams having relatively smaller zone sizes. Since results for the 100mm beams fell close to the lower limit which was obtained from a condition of zero stress transfer, it is concluded that significantly lower closing stresses exist in fracture zones of these beams when compared with larger beams. This has obvious implications for the notch-sensitivity of small beams.

8. The microcracked zone size obtained from strain profiles was confirmed by ultrasonic measurements which gave slightly lower results - on average the zone size was about 44 per cent of residual ligament depth for all beam sizes.

9. The ultrasonic technique was useful for assessing crack depth via the effect that crack growth has on pulse path length. Increments of path length and pulse time were found to fall directly along a line describing the mean ultrasonic pulse velocity in the material. Slight overprediction of crack depth resulted from pulse time measurements at early stages of crack growth, and slight underprediction at later stages. Crack width was found to have no real effect on ultrasonic measurements.

PART IV FRACTURE FORMULATIONS AND CRITERIA

Chapters 9 and 10 form the final part of the thesis. Chapter 9 consists of three major divisions, due to its length. The intention was to keep together in a single chapter all material dealing with the application of fracture mechanics principles. Linear and non-linear parameters will be considered in the light of the test results. Fracture will be briefly studied using a simple stress model which gives information on average stresses in fracture zones. Fracture toughness in terms of fracture zone stresses will also be discussed. The differences in fracture behaviour due to the various beam sizes is a prominent part of the work. Chapter 10 concludes the thesis, and seeks to summarise major aspects such as research objectives and experimental results It also seeks to assess the implications of the results for concrete fracture testing, and to suggest future research needs.

9 PARAMETERS AND CRITERIA FOR CONCRETE FRACTURE

9.1 GENERAL INTRODUCTION

Historically, the study of fracture in concrete has taken two broad directions:- the first is the study of the physical processes of cracking and cracking mechanisms; the second is the characterisation of fracture by means of suitable parameters, and use of these parameters as fracture criteria. The interrelationship between these two broad fields needs to be kept continually in mind, since parameters will tend to describe different fracture processes with varying degrees of success. This implies that fracture parameters must be chosen to suit fracture processes. In this context, a "fracture process" is defined as the nature of crack extension through a specimen, and the degree of damage accompanying crack extension. Hence, it has to do with the presence, extent, and intensity of microcracking, which will be influenced by most of the major factors affecting fracture such as notch depth, specimen size, crack instability, and energy levels.

At present no single fracture parameter has been universally accepted as being applicable to concrete; indeed it might be that in the end a number of different parameters will have to be selected in order to cover the various fracture processes and design requirements. The chief object of this chapter is to consider a number of fracture formulations and parameters in relation to the tests, and to investigate the validity of their application to concrete. The parameters will be critically tested for their ability to describe concrete fracture, and effects of specimen size and notch depth will be investigated. Ideally for a parameter to be accepted as a fracture criterion, it should give a measure of the fracture resistance of the material which essentially will be

independent of specimen size and geometrical effects. In this case, the fracture criterion is expressed in terms of a limiting or critical value of the relevant parameter. This is analagous to, say, the compressive strength criterion, which is the limiting or critical value of the compressive stress for a material. However, the requirements of an ideal parameter may be unrealistic and impractical for concrete, due to the different fracture processes that occur.

Detailed review and discussion of fracture mechanics parameters and their relevance for cemented materials has been given previously in chapters 2 and 3. Both linear elastic (LEFM) parameters and non-linear (NLFM) parameters were discussed. These broad parametric groups will be dealt with in this chapter, use being made of compliance and fracture zone relationships given in chapters 6 to 8.

This chapter is divided into three as follows:-

DIVISION 1 deals with the application of fracture mechanics principles to concrete, and estimation of crack growth for calculating fracture parameters.

DIVISION 2 is concerned with LEFM parameters, and the influence of compressive strength, notch depth, and beam depth on these parameters. Emphasis will be placed on the stress-intensity parameter K (i.e. K_I, the opening mode stress-intensity factor). Non-linear and quasi-plastic effects will therefore be ignored, and the material will be treated as ideal elastic-brittle. The use of K as a fracture criterion at different stages in the fracture process will be considered.

DIVISION 3 discusses non-linear effects in fracture beams. The effects of microcracked non-linear zones, the existence of which has been well established in the experimental work, will be considered by an examination of stresses in fracture zones and the

variation of these zone sizes during crack growth. The crack-closing stresses in the microcracked zone can be thought of as contributing an additional component to the stress-intensity factor at the tip of an effective crack. This concept will be used in the development of a fracture resistance parameter K_R as a function of crack growth, which is basically the non-linear R-curve approach to fracture. The final section will consider energy parameters and their possible use as fracture criteria. The effective fracture surface energy γ' and a modification of this parameter γ_R will be considered, particularly with reference to specimen size.

Each division is concluded with a summary and critical comment, which are brought together at the end of the chapter for the final concluding section.

DIVISION 1 PRELIMINARY CONSIDERATIONS

9.2 APPLICATION OF FRACTURE MECHANICS PRINCIPLES TO CONCRETE

In chapter 2 (2.5) the question of the application to cemented materials of fracture mechanics principles in general, and LEFM in particular, was discussed. The two basic problems identified were those of notch-sensitivity and minimum specimen size. These two aspects are, of course, related, and this was demonstrated in chapter 5 (5.4) where the present concrete was shown to be notch-insensitive for 100mm deep beams, but notch-sensitive for beams of depth 200mm and greater. Specimen size effects relative to experimental results will be dealt with in more detail later, but first it is necessary to demonstrate the relationship between specimen size, notch depth, and notch-sensitivity.

9.2.1 LIMITING SPECIMEN SIZE

A number of researchers have investigated the relationship between specimen size and notch-sensitivity, among them Walsh[99], Mai et al[43], and Ziegeldorf et al[94]. Walsh was able to show that below a certain critical depth for a notched concrete beam, failure was governed by the net section stress reaching the modulus of rupture, i.e. the material was notch-insensitive; for deeper specimens, he proposed that the linear elastic fracture criterion of $K = K_c$ applied. Unfortunately, Walsh ignored slow crack growth prior to maximum load, which is significant even for larger beams (see 6.7). Consequently, he underestimated the fracture toughness of his concrete beams. He suggested that the depth of a notched concrete beam should be not less than 230mm for the LEFM fracture criterion to apply. Mai et al, working with asbestos cement, used the criterion

of notch-sensitivity to develop an expression showing that, for applicability of LEFM to notched beams, the beam depth should be greater than $4(K_c/f_r)^2$ where K_c is the critical stress intensity factor and f_r is the modulus of rupture. This gives similar values for minimum depth of concrete beams as Walsh obtained. Ziegeldorf et al developed an expression showing that notch-sensitivity was a function of K_c, f_r, and notch depth. This expression was found to explain the initial reduction in net failure stress of notched specimens with increasing notch depth, followed by a subsequent increase as notch depth became very deep. (See figure 2.10). The method of Ziegeldorf et al is developed below, but in a different form in order to demonstrate the important relationship between beam depth, notch depth, and material parameters.

From the development of equation (3.7) we can write:-

$$\frac{K}{\sigma_n} = \left(1-\frac{c}{d}\right)^2 \sqrt{c}\, Y \qquad (9.1)$$

where K is the stress-intensity factor

σ_n is the net stress at the root of the notch

Y is the geometrical correction term from figure 3.4

and c, d are notch depth and beam depth respectively.

Introducing the modulus of rupture (f_r) into equation (9.1) and re-arranging we obtain:-

$$\frac{K}{f_r} = \frac{\sigma_n}{f_r}\left(1-\frac{c}{d}\right)^2 \sqrt{c}\, Y$$

$$\text{or } \frac{\sigma_n}{f_r} = \frac{K}{f_r}\left[\left(1-\frac{c}{d}\right)^2 \sqrt{c}\, Y\right]^{-1} \qquad (9.2)$$

For the condition of notch-sensitivity, and hence the basic requirement for the applicability of fracture mechanics, we have that:-

$\frac{\sigma_n}{f_r} <$, which by substituting K'_c for K in equation (9.2) becomes:-

$$\frac{K'_c}{f_r} < \left(1-\frac{c}{d}\right)^2 \sqrt{c}\, Y \qquad (9.3)$$

where K'_c is some suitable critical value of stress-intensity factor, or fracture toughness.

This expression can be re-arranged in terms of the required minimum depth of the beam as follows:-

$$c > \left(\frac{K'_c}{f_r}\right)^2 \left[\left(1-\frac{c}{d}\right)^2 Y\right]^{-2} \qquad (9.4)$$

and since $d = \frac{c}{c/d}$ we can write:-

$$d > \left(\frac{K'_c}{f_r}\right)^2 \frac{1}{c/d} \left[\left(1-\frac{c}{d}\right)^2 Y\right]^{-2}$$

or $$d > \left(\frac{K'_c}{f_r}\right)^2 \left[g\left(\frac{c}{d}\right)\right]^{-1} \qquad (9.5)$$

where $$g\left(\frac{c}{d}\right) = \frac{c}{d}\left[\left(1-\frac{c}{d}\right)^2 Y\right]^2 \qquad (9.6)$$

Equation (9.5) shows that the minimum beam depth required for applicability of fracture mechanics principles is a function of the ratio of fracture toughness to the modulus of rupture, and the geometry of the notched beam. Equation (9.5) can be expressed graphically by plotting d against c/d for various ratios of (K'_c/f_r). Typical values of (K'_c/f_r) of 0,1, 0,2, 0,3 and 0,4 ($\sqrt{m}$) were chosen, and results are shown in figure 9.1. (Note that values of Y_{eff} from figure 3.4 were used to produce figure 9.1).

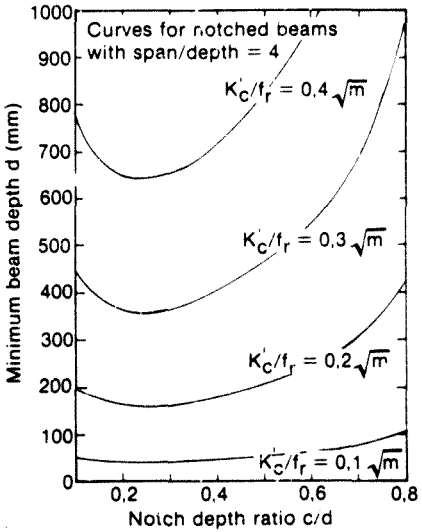

Figure 9.1 Limiting beam depths for notch-sensitivity of fracture beams

Note the following from figure 9.1:-

1. The limiting value for beam depth is critically dependent on the material parameters K'_c and f_r, and an increase in K'_c or a decrease in f_r will require deeper beams to be used. A ratio equivalent to $(K'_c/f_r)^2$ is in fact used in the metallic field to describe the plastic zone size in fracture specimens; limiting specimen dimensions are expressed in terms of the ratio, in order to ensure a valid fracture test. Values of (K'_c/f_r) ranging from 0,1 to 0,4 are not uncommon for cemented materials, and the figure shows the very large beam depths required for tougher materials.

2 Notch depth has a marked influence on minimum beam depth. There is a critical notch depth ratio of about 0,25 giving the

smallest beam depth required for validity of a fracture mechanics approach. However, for notch depth ratios ranging from about 0,2 to 0,4, there is no great practical variation in minimum beam depth.

3. Minimum beam depth increases sharply as notch depth ratio reduces below about 0,15. The condition where modulus of rupture will control failure of the beam, i.e. the unnotched condition, is being approached. Since stress-intensity K is a function not only of global stress but also of crack depth, the influence of the crack diminishes as crack depth reduces. To induce a valid K'_c fracture condition, a deeper beam is therefore required to give a reasonable crack depth.

4. Minimum beam depth increases with increasing notch depth beyond the critical notch depth mentioned above. This reflects the fact that for deep notching the material becomes less notch-sensitive as the net section reduces and a shallow beam condition is approached. (See figure 2.10). Therefore in order for a valid fracture condition to apply for deep notching, a very deep beam is required to ensure sufficient residual beam depth.

5. Referring to figure 5.6, beams of depth equal to or greater than about 200mm were notch-sensitive. Relating this to figure 9.1, it appears that an appropriate (K'_c/f_r) value was approximately 0,22 $\sqrt{m}$ (on the basis of LEFM). An overall average value of f_r for all three series was 4,9MPa, giving an equivalent K'_c value of 1,08MPa$\sqrt{m}$. This value will be compared with measured critical K values in a later section. However, this value does raise the interesting question of exactly which K value should be used to assess whether failure of the specimen is controlled by the notch, or merely by the net section stress. This point is discussed below

9.2.2 INSTABILITY CONDITIONS IN FRACTURE BEAMS

In addition to the requirement of notch-sensitivity, a fundamental requirement for valid fracture testing is that a true condition of fracture instability should occur. This is the inherent requirement in Griffith's equation (2.2), and expresses the fact that there should be a degree of spontaneous crack growth or unstable crack propagation for the Griffith fracture criterion to be valid. According to the extension of the simple Griffith model by the Glucklich model for heterogeneous materials (see figures 2.4 and 2.5), such unstable crack growth may be arrested many times during a test as fracture toughness increases with crack growth. This is the condition normally applying to concrete where further external energy is required beyond maximum load to induce full fracture. The point to be stressed is that measured fracture toughnesses will differ as the condition of crack instability is met or not. For deeply notched beams (say $c/d \geq 0,5$) the energies pertaining during a fracture test are usually insufficient to drive the crack in an unstable manner. Therefore the measured fracture toughness will not be the same as when spontaneous crack advance has occurred, such as in shallower notched beams. This point will be demonstrated later in this chapter when the effects of deep notching are discussed.

Referring to a typical test record such as figure 4.6(a), there are at least three distinct points or regions for which different K values can be calculated:-

1. The point of departure from linearity, on the initial rising branch of the load-deflection curve. This is identified as the point of tangency between the test record and the line representing the initial compliance λ_0. Mai et al[83] maintain that for asbestos cement this departure point may be regarded as the condition of fracture initiation, i.e. that point at which the first measurable crack advance occurs. For concrete beams, this point more likely represents the condition for which appreciable development of the microcracked zone begins, and

there is no main crack advance until some later point on the record. Nevertheless, whether crack advance occurs in real terms or as an extension of the effective crack, this point marks the condition where the fracture process begins. For the present work, K evaluated at this point is termed K_0.

2. The point of maximum load, sometimes termed the point of maximum load instability. This latter term may be misleading, however, since true instability (i.e. spontaneous crack propagation) may or may not occur at this point, depending primarily on the notch depth. For the present tests, beams with $c_0/d = 0,5$ were found to have no true spontaneous crack advance either at this point or at any other point in the test record. Shallower notched beams generally exhibited crack instability at this point, the degree of instability increasing as c_0/d decreased. Main crack advance generally occurred prior to maximum load, and the microcracked zone had developed to its full extent before this point. Hence, for beams with $c_0/d = 0,2$ to $0,4$, this point could be taken as representing a true condition of fracture instability. However, it was not necessarily the first point at which instability could have been measured. For the present work, K evaluated at this point is termed K_c, in order to be consistent with general usage of this term. However, it should not be confused with the more general usage of K'_c in figure 9.1 as some suitable critical value of K.

3. The general region beyond maximum load, on the descending branch of the load-deflection record. The load-cycling technique showed that, particularly for the first few cycles after maximum load, a condition of crack instability occurred at the peak of each cycle. Crack extension leading to final fracture did not necessarily occur at these points, although this did occur on a number of occasions. Rather, crack instability was more incipient in that slow crack extension occurred, as also shown in figure 4.6(a). Sufficient energy to drive the crack existed at these points, which could therefore be regarded as representing conditions of true fracture instability. K values calculated at these points are termed K_R for the present work.

Such calculations form the basis of the K_R-curve approach. (i.e. a form of the R-curve) dealt with in more detail in 9.13. K_R values can substantially exceed K_0 and K_m values.
(One further point, the point of initiation of main crack extension characterised by K_i, will be defined later in 9.13).

The different K values discussed above illustrate the difficulty of using a purely LEFM approach to fracture of cemented materials. Each K value represents a distinct phase within the overall fracture process. The fact that K values increase with crack growth violates the purely Griffith approach in which full and final fracture occurs at initial crack instability. Therefore, a clear understanding is required of which phase of the fracture process is being examined, and an appropriate K value selected. Referring to figure 9.1, it is not easy to decide which K value (i.e. K_0, K_c, or K_R) is appropriate for substituting for the critical value, K'_c. Part of the problem lies in the fact that figure 9.1 is based on an analysis which assumes full fracture instability when a critical K value is reached, which is not true for concrete (although it may be true for hardened cement paste). Therefore we can only use figure 9.1 as a general guide in deciding on minimum beam depth for applicability of fracture mechanics. As a first estimate, it is suggested that the K value for fracture initiation, i.e. K_0 be applied to figure 9.1, although fundamentally a value such as K_c may also be appropriate. This will be discussed later in the chapter.

9.2.3 INFLUENCE OF MATERIAL HETEROGENEITY

Previous discussion has shown that LEFM is not easily applicable to concrete beams. It is also necessary to consider how concrete as a highly heterogeneous material relates to the concepts of fracture mechanics. LEFM assumes an elastic, homogeneous and isotropic medium, from which concrete is far removed. For very large specimens where aggregate size is small in relation to specimen dimensions, concrete may be regarded as approaching the LEFM

Author Alexander Mark Gavin
Name of thesis Fracture Of Plain Concrete: A Comparative Study Of Notched Beams Of Varying Depth. 1985

PUBLISHER:
University of the Witwatersrand, Johannesburg
©2013

LEGAL NOTICES:

Copyright Notice: All materials on the University of the Witwatersrand, Johannesburg Library website are protected by South African copyright law and may not be distributed, transmitted, displayed, or otherwise published in any format, without the prior written permission of the copyright owner.

Disclaimer and Terms of Use: Provided that you maintain all copyright and other notices contained therein, you may download material (one machine readable copy and one print copy per page) for your personal and/or educational non-commercial use only.

The University of the Witwatersrand, Johannesburg, is not responsible for any errors or omissions and excludes any and all liability for any errors in or omissions from the information on the Library website.